Distribution Agreement

In presenting this thesis or dissertation as a partial fulfillment of the requirements for an advanced degree from Emory University, I hereby grant to Emory University and its agents the non-exclusive license to archive, make accessible, and display my thesis or dissertation in whole or in part in all forms of media, now or hereafter known, including display on the world wide web. I understand that I may select some access restrictions as part of the online submission of this thesis or dissertation. I retain all ownership rights to the copyright of the thesis or dissertation. I also retain the right to use in future works (such as articles or books) all or part of this thesis or dissertation.

Signature:

Kawai Leung	Date

INFERRING CHARACTERISTICS OF SENSORIMOTOR BEHAVIOR BY QUANTIFYING DYNAMICS OF ANIMAL LOCOMOTION

By

Kawai Leung
Doctor of Philosophy

Physics

Ilya Nemenman, Ph.D
Advisor

Gordon J. Berman, Ph.D
Committee Member

Stefan Boettcher, Ph.D
Committee Member

Minsu Kim, Ph.D
Committee Member

William S. Ryu, Ph.D
Committee Member

Accepted:

Lisa A. Tedesco, Ph.D
Dean of the James T. Laney School of Graduate Studies

Date

INFERRING CHARACTERISTICS OF SENSORIMOTOR BEHAVIOR BY QUANTIFYING DYNAMICS OF ANIMAL LOCOMOTION

By

Kawai Leung
M.Sc., The Chinese University of Hong Kong, 2011
B.Sc., The Chinese University of Hong Kong, 2010

Advisor: Ilya Nemenman, Ph.D

An abstract of
A dissertation submitted to the Faculty of the
James T. Laney School of Graduate Studies of Emory University
in partial fulfillment of the requirements for the degree of
Doctor of Philosophy
in Physics
2017

Abstract

INFERRING CHARACTERISTICS OF SENSORIMOTOR BEHAVIOR BY QUANTIFYING DYNAMICS OF ANIMAL LOCOMOTION

By Kawai Leung

Locomotion is one of the most well-studied topics in animal behavioral studies. Many fundamental and clinical research make use of the locomotion of an animal model to explore various aspects in sensorimotor behavior. In the past, most of these studies focused on population average of a specific trait due to limitation of data collection and processing power. With recent advance in computer vision and statistical modeling techniques, it is now possible to track and analyze large amounts of behavioral data. In this thesis, I present two projects that aim to infer the characteristics of sensorimotor behavior by quantifying the dynamics of locomotion of nematode *Caenorhabditis elegans* and fruit fly *Drosophila melanogaster*, shedding light on statistical dependence between sensing and behavior.

In the first project, I investigate the possibility of inferring noxious sensory information from the behavior of *Caenorhabditis elegans*. I develop a statistical model to infer the heat stimulus level perceived by individual animals from their stereotyped escape responses after stimulation by an IR laser. The model allows quantification of analgesic-like effects of chemical agents or genetic mutations in the worm. At the same time, the method is able to differentiate perturbations of locomotion behavior that are beyond affecting the sensory system. With this model I propose experimental designs that allows statistically significant identification of analgesic-like effects. In the second project, I investigate the relationship of energy budget and stability of locomotion in determining the walking speed distribution of *Drosophila melanogaster* during aging. The locomotion stability at different age groups is estimated from video recordings using Floquet theory. I calculate the power consumption of different locomotion speed using a biomechanics model. In conclusion, the power consumption, not stability, predicts the locomotion speed distribution at different ages.

INFERRING CHARACTERISTICS OF SENSORIMOTOR BEHAVIOR BY QUANTIFYING DYNAMICS OF ANIMAL LOCOMOTION

By

Kawai Leung
M.Sc., The Chinese University of Hong Kong, 2011
B.Sc., The Chinese University of Hong Kong, 2010

Advisor: Ilya Nemenman, Ph.D

A dissertation submitted to the Faculty of the
James T. Laney School of Graduate Studies of Emory University
in partial fulfillment of the requirements for the degree of
Doctor of Philosophy
in Physics
2017

Acknowledgement

First of all, I would like to thank my advisor, Dr. Ilya Nemenman, for his guidance and support during these years. I learn a lot from his knowledge in almost everything, including physics, statistics, biology and occasionally, geography and history. I enjoyed my time working with him, as I always get to learn something new. He influenced me in many aspects in my life, and he will always be a role model in my career.

I am very grateful to my collaborator, Dr. William S. Ryu. Will is an excellent scientist and a great mentor. He introduced me to the wonderful world of Biophysics and helped me through the toughest time in our project. His knowledge and vision always inspire me. Also, I would like to thank Dr. Aylia Mohammadi who collected data for our project.

I would also like to thank my collaborator, Dr. Gordon J. Berman. He is a nice person, has a good sense of humor, and it is very rewarding to work with him. Also, I would like to thank my dissertation committee member, Dr. Stefan Boettcher, and Dr. Minsu Kim. Your advice guided me to finish my research projects.

I would like to thank all the people in Emory Physics department. Dr. Vijay Singh, Dr. Xinxian Shao, Dr. David Hofmann, Dr. Andrew Mugler, Dr. Damian Hernandez Lahme, Baohua Zhou, Catalina Rivera, Joe Natale, and other members of Nemenman Lab have been very helpful and supportive. Jason Boss, Art Kleyman, Calvin Jackson, Barbara Conner and Dr. Connie Roth helped me to navigate through the maze of school bureaucracy.

Across the globe, I would like to thank my family in Hong Kong. My parents have been very supportive and gave me the freedom to pursue a Ph.D. degree. Without their help, I would never be able to finish. Last but not least, I thank my fiance, Poying Lai for accompanying me on this intellectual adventure for the last ten years. I could not be more grateful for your support and patience.

Table of Contents

List of Figures

List of Tables

Chapter 1 Introduction

Animal locomotion has been one of the most studied topics in biology. Since the beginning of natural science, scientists and philosophers have been dedicated to explore the relationship between sensation and locomotion. In *Movements of Animals*, one of the earliest studies of biology, Aristotle discussed and proposed a qualitative model of sensing and locomotion [1]. Inevitably, he was incorrect - and so were many researchers after him. The main reason behind this failure is that unlike other in other disciplines, it was impossible at the time to quantify and characterize the full repertoire of behavior and sensory input of an animal. But in the last several decades, with the advance of computer vision and data analysis techniques, we are now able to capture and analyze a significant amount of behavioral data from multiple animals. At the same time, we are also able to deliver precise stimulation to the sensory system. Combined with automated data collection, it is now possible to collect large quantitative stimulus to behavior datasets, which opens up a way to investigate the relationship between sensory input and animal behavior. In the following thesis, I present two projects that are related to inferring characteristics of sensorimotor behavior by quantifying the locomotion of the nematode *Caenorhabditis elegans* and the fruit fly *Drosophila melanogaster*.

The nematode *C. elegans* was proposed as a model organism in genetics and neuroscience in the second half of twentieth century [2]. Since then, it has been used in different disciplines such as cell biology, neurobiology and aging [3, 4]. Many important discoveries in biomedical science were first made in the worm [5]. The worm has a number of features that make it an important tool in biomedical or basic biology research, especially for studies in sensorimotor behavior. First, it is easy to be raised and maintain in a laboratory setting on a diet of *E. coli*. Second, the rapid

reproduction and growth facilitate large-scale experiments on this animal. Third, the transparent nature of the worm body allows the use of *in vivo* fluorescence markers to study biological process. Fourth, although the nervous system is relatively simple, with only 302 neurons, the worm exhibits complex behavior [6, 7]. These qualities make *C. elegans* an ideal model to study the sensorimotor behavior.

The locomotion behavior of *C. elegans* has been very well studied. In early studies, standard assays for behavior were subjective and imprecise. For example, uncoordinated mutants ("Unc") are classified qualitatively into categories such as "Coiler", "Irregular movement", "Shaker" and "Sluggish" [8]. Since these categories are vague and subjective, it is not surprising that the quantitative relationship of sensory information and locomotion behavior remained unexplored for several decades. It was not until the last 20 years that the behavior of the worm could be quantitatively characterized [9, 10]. Many different methods have been designed to study unconstrained locomotion using video microscopy [11, 12, 13, 14]. These methods reveal important features of worm locomotion, such as low dimensional shape space [15] and stereotyped behavior [16]. Base on these results, we are able to develop a statistical model of behavior through quantifying locomotion.

The worm has been shown to react to chemical, mechanical and thermal stimuli [17, 18, 19]. It is also a very well established model organism in the study of nociception [20]. Despite these efforts, no method allows us to infer to perceived noxious level from single worm behavior. In most of these studies, the nociception assays focus on a particular behavioral feature of the subject, which is usually selected in an ad hoc fashion. At the same time, these assays may convolve the effect on the sensory system to motor behavior. To address these problems, I present a quantitative model to infer the perceived level of pain from stereotypical escape response of *C. elegans* stimulated by an IR laser in Chapter 2. The model provides a method for quantification of analgesic-like effects of chemical stimuli or genetic mutations in *C. elegans*. I

test the model with Ibuprofen-treated worms, and I show that the ibuprofen lowered the perceived level of pain significantly. At the same time, by assuming a stereotypical escape behavior, this model can differentiate between the effect of chemical of mutation beyond the thermal sensory system.

The fruit fly *D. melanogaster* is another common model organism. In particular, it is used as a model in genetics [21], aging [22] and behavior [23]. Since flies have a relatively short life span and are inexpensive to maintain, it is a perfect model for studying functional decline during aging. Many aspects of age-related functional decline were studied in this animal, such as geotaxis [24], exploratory activity [25], olfaction [26] and cardiac function [27]. Many of these functional declines are related to the distribution of locomotion speed. On average, the animal moves slower during aging. There are two explanation for this effect - reduction of energy budget [28] and ability of motor control [29].

In Chapter 3, I present a project that aims to find out the the relationship between *D. melanogaster* locomotion speed distribution, the energy cost of transport and stability by quantifying locomotion at different ages. Estimating the energy budget and ability of motor control is not a trivial task, but previous research has already paved the way to our goal. First of all, the fly has to be tracked and analyze automatically. Development of Computer Vision offers an effective strategy for automatically tracking and measuring the behavioral phenotype of flies [30, 31, 32]. Second, the energy cost of locomotion can be estimated by a biomechanical model [33, 34]. Finally, the stability of locomotion can be estimated through Floquet theory [35, 36]. I discover that the energetic cost of transport, not stability, significantly predicts the speed distribution during aging.

Chapter 2 Stereotypical escape behavior in *Caenorhabditis elegans* allows quantification of effective heat stimulus levels

2.1 Introduction

A *grand goal* in understanding sensory systems is to predict the behavioral response of an organism to specific sensory stimuli; or, conversely, to infer the sensory stimuli from measurements of the behavioral response. Such a goal requires careful experimental design, precise control of the sensory inputs, and quantification of the behavioral outputs. While sensory stimuli can be carefully quantified and applied, the quantification of the behavioral output and its relationship to the stimulus is non-trivial because the behavior is often complicated and not well defined. In this work we address this grand goal in the context of studies of pain, or nociception (i. e., sensing of noxious stimuli, which damage or threaten to damage normal tissues), where behavioral quantification is especially hard. (Note that, in this paper, we use nomenclature developed by the International Association for the Study of Pain, http://www.iasp-pain.org/Taxonomy.)

Pain studies on human subjects are difficult because of ethical constraints, difficulties in quantifying a psychophysical response, and subjectivity in self-reporting [37]. Partial conservation of molecular mechanisms of nociception among many different species [38, 39, 40] allows to solve some of these problems by using animal models. However, then the grand goal of quantifying the behavior and relating it to the stimulus becomes even harder: animal subjects cannot communicate their perceived noxious levels to us in an obvious fashion. Thus progress in using animal models depends crucially on our ability to quantitatively and objectively infer the perceived

level of noxious stimuli from animal behavior.

Historically, studies of nociception primarily used mammalian models [41, 42]. For rodents, the tail flick test [43], the hot-plate test [44, 45] and the Hargreaves' method [46] correlate pain perception with the reaction latency of different body parts to noxious stimuli. For larger animals such as canines [47] and primates [48, 49], similar nociceptive assays have also been developed. In recent years, new approaches started incorporating facial expressions in nociception quantification [50, 51, 52]. Although these mammalian models are extensively studied, several drawbacks hinder their use. First, ethical issues and risks arise for certain experiments. Second, compared to invertebrates, vertebrate subjects require more time and resources to maintain. Therefore, much effort has been devoted to investigations of the possibility of using invertebrate models in nociception research [39, 53]. In experiments involving *Drosophila* larva, measures such as the response percentage of the total population [54, 55] and the time to response [56] have been used to investigate changes in the ability of the animals to sense noxious stimuli. In experiments on *Caenorhabditis elegans*, behavioral features such as the turning rate [38] and the percentage of escape response [57] have been used to characterize nociception.

All of these models share some common problems. First, the nociceptive assays focus on one particular coarse behavioral feature of the subject, such as avoidance behavior, orientation, or turning rate. Such features are selected in an ad hoc fashion, subject to a particular design of an experiment. This makes it difficult to compare results across different labs and experiments. Further, this does not solve the grand goal of quantifying the full stimulus-behavior relation, and thus the behavior may be providing additional information about the perceived noxious stimulus level that is not being captured by the coarse measures. Second, some assays report measurements as a percentage of a population, so that these measurements cannot be made for individuals. To overcome these problems, an ideal assay would infer a perceived noxious

stimulus level of an individual animal on a continuous scale, using comprehensive, objective measurements of its behavioral profile.

Solving the grand goal of quantifying the stimulus-behavior relation in the context of pain studies would allow one to use the assays to calibrate the perceived noxious stimulus level, and maybe even reductions in such levels due to analgesic-like effects of drugs, or mutations in the nociceptive pathways. At the same time, drugs or mutations can affect the motor response, rather than the nociception per se. Thus traditional pain assays mentioned above may convolve the perceived noxious stimulus reduction, if any, with behavioral changes. For example, a mutant defective for turning behavior will register a strong reduction in the turning rate, but it would be a mistake to interpret this as a reduction in nociception. Such concerns are very real, as is illustrated by a known fact that opioids can cause large behavioral changes [58]. To attribute a behavioral response difference to reduced nociception and not to motor changes, the response must be stereotyped and reflexive, which is often the case [42]. Further, only the response amplitude or frequency, but not the detailed temporal structure, should change in response to a drug or a mutation. Establishing the stability of the stereotypic response pattern requires solving the grand goal: analysis of the *entire stimulus-triggered response behavior*, rather than of its few selected features, as is done by most behavioral assays.

In this work, we address these issues in the context of the nematode *C. elegans*, solving the grand goal in the context of its heat-evoked escape behavior, and hence developing the worm further as an animal model system for nociception research. The worm is a great model organism for such studies for a number of reasons. First, the behavioral dynamics of freely moving *C. elegans* is intrinsically low dimensional [15]. This makes quantification of its behavioral response relatively straightforward, providing an opportunity to use the entire motile behavior as a basis for assays. Second, the worms show a noxious response to a wide range of sensations including

certain types of chemical [59, 60], mechanical [61, 18], and thermal [62, 63] stimuli, and such a nociceptive response is different from and is transduced independently of the related taxis behaviors [64, 65, 66, 67, 68]. Third, at the molecular level, many details of heat nociception in the worm may be similar to vertebrate animals [39]. Fourth, there are powerful genetic and optical tools to reveal mechanisms of nociception in *C. elegans*. Finally, the low cost, small size, and absence of ethical constraints make the animal amenable to large scale pharmacological screens for new human analgesics [69].

We present combined experimental and modeling studies that show that the entire temporal behavioral profile during the heat-evoked escape response in *C. elegans* is highly stereotypical, with the frequency of the escape response and the amplitude of the escape velocity profile scaling with the stimulus level. By verifying the ability of the behavioral template to capture the response following a heat stimulus, the model we develop distinguishes changes in sensory system from changes to the motor program. When a change is attributed to the sensory system, the model can infer the reduction in the perceived heat stimulus level following pharmacological or genetic treatments from the behavior of an individual worm. This quantification requires only about 60 worms to show statistically significant perceived stimulus reduction for a common human analgesic, and its statistical power quickly improves with an increasing number of subjects.

Overall, this solution of the grand goal in the worm heat-evoked escape context suggests that, for *C. elegans*, it is possible to disambiguate perturbations to the sensory system from other perturbations affecting motility, and to quantify the reduction in the perceived heat stimulus from behavioral data. Combined with the previous evidence, this bodes well for further establishment of the worm as a model system for pain research. However, we stress that the differences between the worm and the human are so large that we do not want to overstate the importance of a *C. elegans*

nociception model in the study of human health. Our analysis may be useful in the future for identifying molecular mechanisms of nociception (which may be similar to those leading to pain in humans), or identification of drugs that affect them. Some of these drugs may even work in humans, but there is no reason to believe that pain (and especially its emotional component) occurs in *C. elegans*, or that drugs that affect nociception actually produce analgesic effect in worms. Thus the main contribution of our work is in addressing the *grand goal*, namely in quantitative characterization of regularities of complete heat-evoked escape behavior *C. elegans* on a single-subject level, and analysis of changes in these regularities under different pharmacological and genetic treatments, rather than potential applications of our findings to future discovery of new human analgesics.

2.2 Results

We aim to infer the perceived heat stimulus level from the temporal dynamics of the worm response. The heat stimulation is administered using an infrared laser while the worm crawls on an agar plate. The worm motion is captured by video microscopy and analyzed using custom image analysis software. The worm postures are very stereotypical, adding up to simple sinusoidal motions forwards or backwards, and to turns [15]. Thus without much loss of the statistical power, we characterize the entire escape behavior of the animal by a time series of its center of mass velocity (*Materials and Methods*). Our task is then to verify if such responses are stereotypical, scaling in frequency and amplitude with the applied laser current. If they are stereotypical and thus can be used to characterize the perceived stimulus level, the next task is to infer the applied laser current from the velocity data.

For each heat stimulus trial a random worm is selected on the plate and its motion is sampled at 60 Hz for 15 s. An infrared laser pulse with a randomly chosen current between 0 to 200 mA and a duration of 0.1 s is then directed to the head of the worm

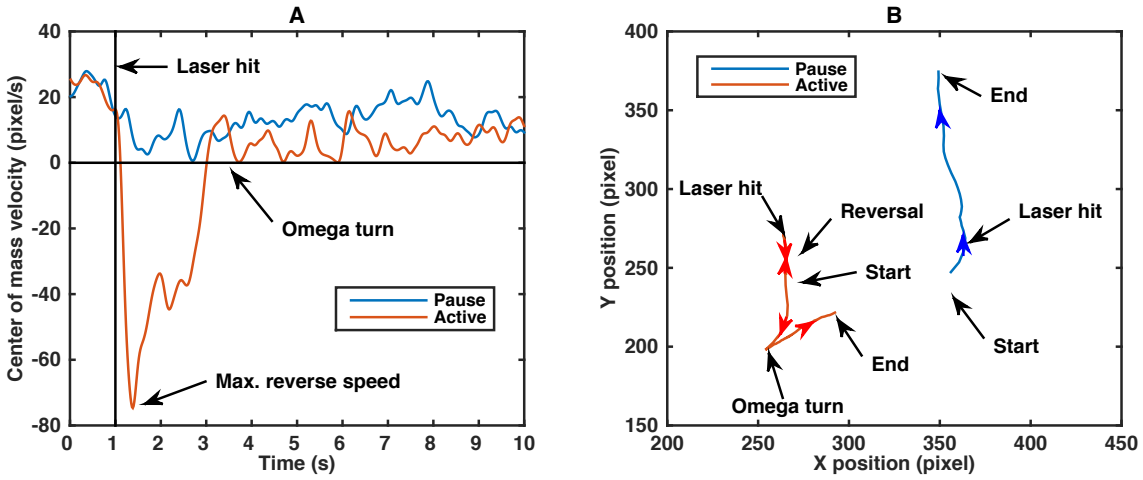

Figure 2.1: Typical center-of-mass heat-evoked escape responses in *C. elegans*. (A) Typical center-of-mass trajectory of two wild-type worms in a paused and an active state (see below for the detailed discussion of the two states). The infrared laser was directed at each worm at $t = 1$ s. The paused state is characterized by the near zero velocity after the laser stimulus. (B) Actual trajectories of these two worms. Worm changes its direction of motion in two ways: in a "reversal", it stops and backtracks along its previous path; in an "omega" turn the worm's head curls back and crosses the tail, setting then a new direction of forward motion.

1 s after the start of the video recording. The worm's center of mass motion in a typical trial consists of a forward motion before the stimulus, a stop and/or backward motion after the stimulus, then followed by an "omega" turn, after which the worm emerges with a forward motion in a different direction (Fig. 2.1). This is a typical response to many noxious stimuli in *C. elegans*, and not just to heat stimulus [63] (stereotyped, typical escape responses also exist in other animals [70, 71]). Further, previous research has shown that, even though the maximum temperature change in this assay is rather small ($\sim 1 - 2°$C), the escape behavior is significantly different from the more commonly studied thermotactic behavior, and is mediated by different neural and genetic pathways [62, 72, 63].

To understand the effects of pharmacological and genetic interventions , we collected three distinct datasets. In the first, the stimulus was applied to wild-type worms (N2). In the second, the wild-type worms were pre-treated with an ibupro-

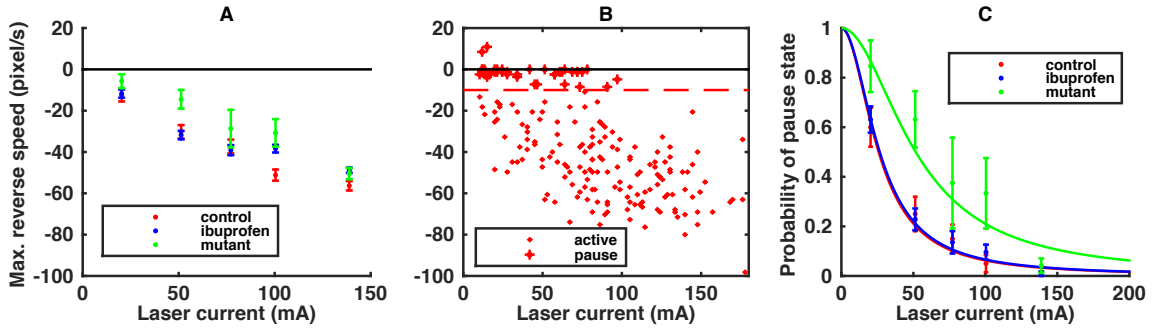

Figure 2.2: Global characteristics of the heat-evoked escape. (A) The mean (± s. e. m.) of the maximum reverse speed for the three worm types is plotted against the stimulus laser current, partitioned into five bins. Negative values correspond to backward motion. (B) Maximum reverse speeds for individual control worms. We define an active worm (dot) as having the maximum reverse speed of over 10 pixels/s (about 0.2 body length per second); otherwise the worm is paused (plus sign). (C) Probability of the paused state vs. the laser current. Dots represent the actual data (± s. e. m.), and lines are the fitted model. The datasets are divided into equally sampled bins for each worm type.

fen solution (*Materials and Methods*), which we surprisingly discovered to affect the heat-evoked response, after screening some common human analgesics. Since ibuprofen's molecular mechanism of action in *C. elegans* is unclear, we refer to this as an analgesic-like treatment throughout the paper. In the third, we applied the stimulus to an untreated triple mutant (ocr-2(ak47) osm-9(ky10) IV; ocr-1(ak46)), which is widely used in *C. elegans* nociception studies; it has one of the strongest effects on reduction of heat-evoked nociceptive response [72]. Hereafter we refer to these datasets as "control", "ibuprofen", and "mutant", respectively. We chose not to explore hyperalgesic treatments for this study. We collectively refer to ibuprofen and mutant worms as "treated" worms. Forward motion in all three data sets was similar (typical forward velocity of 13 ± 9, 9 ± 7, 13 ± 10 pixel/s respectively, where the error denoted the standard deviation of the velocity distribution), so that there are no drastic defects in motility.

2.2.1 Statistical model of the heat-evoked escape

For presentation purposes, we bin the laser current of the heat stimulus into five distinct levels (bins), defined to have an equal number of control worms in each bin (40 per bin). The maximum reverse escape velocity is indistinguishable among all three worm types for the largest stimulus level, indicating no gross defects to motility or noxious response. At the same time, the velocity at smaller stimuli levels shows substantial differences (Z scores of up to 3.8) between the control and the treated worms, especially in the vicinity of $\sim$ 100 mA laser stimulation (Fig. 2.2A). Two way ANOVA shows the difference between the ibuprofen and the control worms at $p = 0.021$ and between the mutant and the control at $p = 1.5 \cdot 10^{-5}$ across all five laser current groups. Mutant worms are especially different from the control over a wider stimulus range. However, as discussed above, it is unclear if such simple observed behavioral differences are indicative of the reduction of the perceived stimulus level or of other changes to the motor response. Furthermore, there might be additional changes in the detailed temporal structure of the heat-evoked escape dynamics, which would not be captured by simple statistics, such as the maximum reverse speed.

To address this, instead of subjectively segmenting the complex escape behavior or choosing *ad hoc* metrics of the worm's movement, we choose to infer the applied stimulus strength from a comprehensive model of the entire worm's response velocity profile. Due to the considerable randomness and individual variability of responses, we choose to model them probabilistically (see [73] for another example of Bayesian probabilistic modeling of nociception). Thus we are interested in estimating $P(I|\mathbf{v})$, the probability distribution of the applied laser current I conditional on the observed velocity of the escape response $\mathbf{v} \equiv \{v(t)\}$. Using Bayes' theorem, we write

$$P(I|\mathbf{v}) = \frac{P(\mathbf{v}|I)P(I)}{P(\mathbf{v})} = \frac{1}{Z}P(\mathbf{v}|I)P(I), \tag{2.1}$$

where Z is the normalization factor, and $P(I)$ is the prior distribution of stimuli.

When we characterize the velocity profiles of the noxious response of *C. elegans*, we notice that the worm can react to the stimulus in two different ways. Some worms pause after the heat stimulus, even at large laser currents (Fig. 2.2B). These worms remain largely immobile for a few seconds, sometimes as long as the recording duration. Other worms actively reverse and follow the classic escape behavior (Fig. 2.1). We choose to separate the active vs. the paused worms with a cutoff of 10 pixels/s, where 50 pixels is about one body length of the worm. To account for this heterogeneity in the behavior, we introduce the state variable s, which can take one of two values, a or p, for each individual worm. Then

$$P(\mathbf{v}|I) = P(\mathbf{v}|s=p,I)P(s=p|I) + P(\mathbf{v}|s=a,I)P(s=a|I). \tag{2.2}$$

We model the probability of the paused state $P(p|I)$ by a sigmoid function (Fig. 2.2C),

$$P(s=p|I,\mathcal{I}_0) = \frac{1}{1+(I/\mathcal{I}_0)^2}, \tag{2.3}$$

where $\mathcal{I}_0$ is the *pause current* threshold. Then the probability of the active state is

$$P(s=a|I,\mathcal{I}_0) = 1 - P(s=p|I,\mathcal{I}_0) = \frac{(I/\mathcal{I}_0)^2}{1+(I/\mathcal{I}_0)^2}, \tag{2.4}$$

We infer $\mathcal{I}_0$ from data by maximizing $\prod_{i=1}^{N_{\text{type}}} P(s_i|I_i,\mathcal{I}_0)$, where N_{type} is the number of trials with worms of the analyzed type, and I_i is the actual laser current for a particular trial. Note that each of the three data sets has its own pause current (25.9 ± 2.8, 26.6 ± 1.9, and 51.6 ± 6.3 mA for the control, ibuprofen, and mutant worms, respectively). Changes in this threshold, like that for the mutant, will result in different numbers of worms responding to the same stimulus, which can be consistent with the changes in the stimulus level, depending on whether the response profiles themselves stay stable. This is what we investigate next. Parenthetically, we note that the fraction of active worms is essentially the same as the percentage of the escape response, which has been used previously to quantify worm nociception [57].

Here we go further and additionally analyze the behavioral profiles of the responding worms.

C. elegans locomotion consists of a series of stereotyped postures and behavioral states [16, 74]. Further, in other animals, escape responses are stereotyped as well [42]. Therefore, it is natural to explore if the escape response of *C. elegans* is also stereotyped, separately for the paused and the active states. For paused worms, the escape velocity is small and independent of the laser current, and we model it as a multivariate normal variable,

$$P(\mathbf{v}|p,I) = \frac{1}{(2\pi)^{\frac{T}{2}}|\Sigma_p|^{\frac{1}{2}}} \exp\left[-\frac{1}{2}(\mathbf{v}-\mathbf{u}_p)^{\mathrm{T}}\Sigma_p^{-1}(\mathbf{v}-\mathbf{u}_p)\right], \tag{2.5}$$

where $\mathbf{u}_p$ is the mean velocity profile of the paused worms measured from data, which we call the *paused template* velocity. Σ_p is the empirical covariance of the paused velocity, and T is the total number of effectively independent time points in the velocity profile time series, determined using the autocorrelation structure of the profile (*Materials and Methods*).

We expect that, in the active state, the worm escape is laser current dependent. Specifically, we seek to represent it by a current-dependent rescaling of a stereotypical escape velocity, $\mathbf{v} \sim f(I)\mathbf{u}_a$, where f is the scaling function, and $\mathbf{u}_a$ is the *active template* velocity. Since various features of the worm escapes (the maximum reverse speed, the maximum reverse acceleration, and the time to the omega turn), scale non-linearly and saturate with the laser current (Fig. 2.2A), the rescaling, $f(I)$, must be sigmoidal. Further, some worms have nonzero velocities even at zero laser current, so that $f(0)$ may be nonzero. Finally, the overall scale of the template can be absorbed in the definition of $\mathbf{u}_a$. The simplest scaling function obeying these constraints has only two parameters

$$f(I) \equiv f_{\mathcal{I}_1,\mathcal{I}_2}(I) = \mathcal{I}_1 + \frac{I}{1+I/\mathcal{I}_2}, \tag{2.6}$$

where $\mathcal{I}_1$ and $\mathcal{I}_2$ are again constants, different for the three different worm types. With this, we write the probability of a velocity profile given the laser current I for

the worm in an active state as a multivariate normal distribution

$$P(\mathbf{v}|a,I)=\frac{1}{(2\pi)^{\frac{T}{2}}|\Sigma_a|^{\frac{1}{2}}}\times\exp\left[-\frac{1}{2}(\mathbf{v}-f_{\mathcal{I}_1,\mathcal{I}_2}(I)\mathbf{u}_a)^{\mathrm{T}}\Sigma_a^{-1}(\mathbf{v}-f_{\mathcal{I}_1,\mathcal{I}_2}(I)\mathbf{u}_a)\right], \quad (2.7)$$

where Σ_a is the covariance of the average velocity profile. We find the constants $\mathcal{I}_1$ and $\mathcal{I}_2$, $\mathbf{u}_a$ and Σ_a by maximizing the likelihood of the observed data (*Materials and Methods*).

In summary, the probability of a velocity profile given the laser current in a certain trial is

$$\begin{aligned}P(\mathbf{v}|I)=&\left\{\frac{1}{1+(I/\mathcal{I}_0)^2}\times\frac{1}{(2\pi)^{\frac{T}{2}}|\Sigma_p|^{\frac{1}{2}}}\exp\left[-\frac{1}{2}(\mathbf{v}-\mathbf{u}_p)^T\Sigma_p^{-1}(\mathbf{v}-\mathbf{u}_p)\right]\right\}\\&+\left\{\frac{(I/\mathcal{I}_0)^2}{1+(I/\mathcal{I}_0)^2}\times\frac{1}{(2\pi)^{\frac{T}{2}}|\Sigma_a|^{\frac{1}{2}}}\exp\left[-\frac{1}{2}(\mathbf{v}-f_{\mathcal{I}_1,\mathcal{I}_2}(I)\mathbf{u}_a)^T\Sigma_a^{-1}(\mathbf{v}-f_{\mathcal{I}_1,\mathcal{I}_2}(I)\mathbf{u}_a)\right]\right\}.\end{aligned} \quad (2.8)$$

The overall model of the experiment, Eq. (2.1), also includes $P(I)$. To a large extent, this is controlled by the experimentalist, and details are described in *Materials and Methods*.

2.2.2 Is the heat-evoked escape stereotyped?

The model we built assumes a stereotypical escape behavior. Is this assumption justified? Velocities in the paused state are very small (worms barely move). Thus whether the stereotypy assumption provides a good model of the data is determined largely by the stereotypy of the active worms. If the active stereotypical response template exists, then it should be possible to collapse the average velocity profiles onto a single curve by the following transformation

$$\mathbf{v}_{\text{collapse}}=\frac{\mathbf{v}_a}{f_{\mathcal{I}_1,\mathcal{I}_2}(I)}. \quad (2.9)$$

Indeed, the means of different bins collapse relatively compactly, providing evidence for the existence of the stereotypy in active responses (Fig. 2.3). We show the template

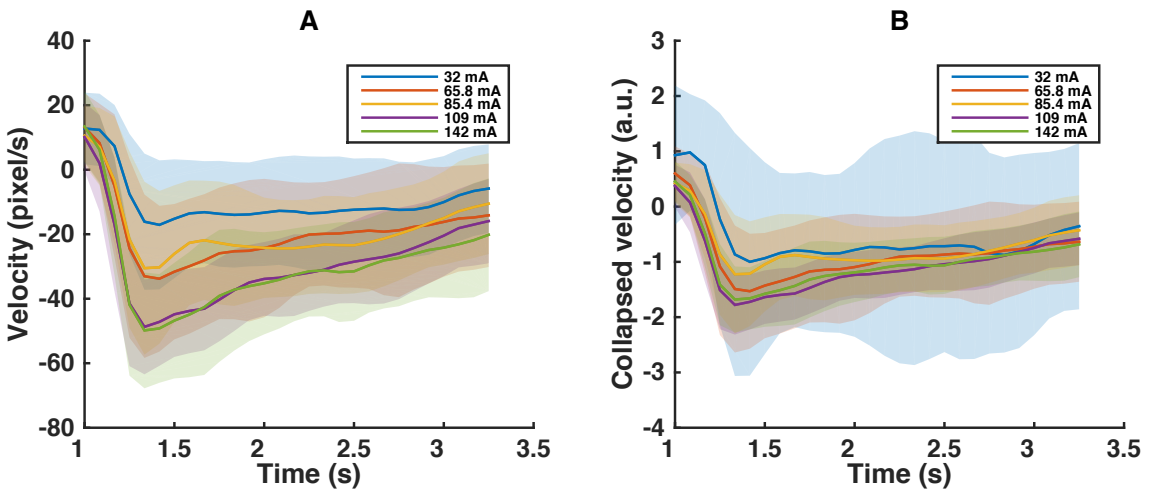

Figure 2.3: Collapse of the response behavior. (A) The mean (dark lines) and standard deviation (similar semitransparent light colors) of velocities of active control worms, binned for presentation purposes into five different groups of 40 worms each, based on the stimulus current. (B) The mean and standard deviation of velocities (same color code) in the same time period rescaled by $f^{-1}_{\mathcal{I}_1,\mathcal{I}_2}(I_i)$. Rescaled mean velocities nearly collapse (see Fig. 2.5 for quantification of the collapse). Note that the parameters $\mathcal{I}_1$ and $\mathcal{I}_2$ are optimized as in *Materials and methods* to collapse individual profiles, and not the five mean profiles illustrated here.

velocities and the non-linear scaling function f inferred from the control, ibuprofen, and mutant in Fig. 2.4.

Note that the three active template velocity profiles are very similar (Fig. 2.4A), but the mutant template velocity profile shows a response lag of 83 ms (one time frame at 12 Hz) compared to the control or ibuprofen data set. In other words, the pharmacological treatments and the mutations weakly affect the templated response, and the mutation slightly delays it. This bodes well for the assumption of the stereotypical response, definitely for ibuprofen and, to a somewhat lesser extent, for the mutant.

While the existence of the stereotypical patterns and their similarity across treatments is encouraging, we still need to quantify how good the statistical models are. In the ideal case, the variance $\boldsymbol{\sigma}^2_{\text{collapse}}$ of the collapsed velocities, Eq. (2.9), calculated over individual trials, would be zero. However, there are a number of expected sources

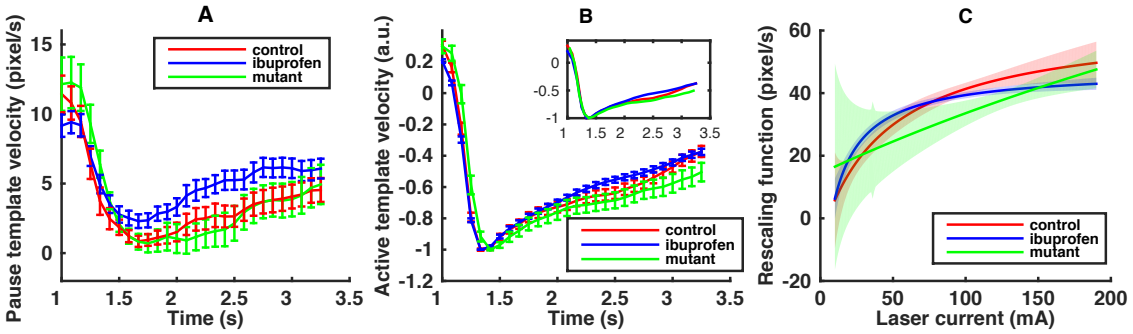

Figure 2.4: Stereotypical active response. (A) Paused template velocities. Error bars show the standard deviation of the template. Models are estimated separately for the three different worm types, indicated by different colors. Time $t = 1$ s corresponds to the moment of the stimulus application. (B) Normalized active template velocity. Each template velocity is normalized by the absolute value of its minimum $|\min_t \mathbf{v}_a|$. The error bars represent the model standard deviation, estimated by bootstrapping (*Materials and Methods*). The subfigure shows the template velocities adjusted by the time of maximum reverse velocity, illustrating that the three templates nearly match. (C) The rescaling function $f_{\mathcal{I}_1,\mathcal{I}_2}(I)$ for the three different worm types, normalized by multiplying by the absolute value of the minimum of the active template velocity $|\min_t \mathbf{v}_a|$. The optimized parameter values are $\mathcal{I}_1 = -4.5, -4.5, 66.5$ and $\mathcal{I}_2 = 45.0, 12.0, \infty$ for the control, ibuprofen, and mutant worms, respectively. We deliberately do not report error bars on individual parameters, but rather show the one standard deviation confidence intervals for the entire rescaling curve as shaded regions on the figure. The confidence region was again estimated using bootstrapping.

of variance in the velocity, such as the individual variability and the model inaccuracies. To establish how good the stereotypical model fits are, we need to disambiguate these contributions. For this, we again partition all velocity profiles into five current bins. We then write the total variance of all responses as

$$\boldsymbol{\sigma}^2_{\text{total}} = \boldsymbol{\sigma}^2_I + \boldsymbol{\sigma}^2_{\text{ind}}, \tag{2.10}$$

where $\boldsymbol{\sigma}^2_{\text{ind}}$ is the variance due to individual responses within each bin, and $\boldsymbol{\sigma}^2_I$ is the current-driven variance of the mean responses across the bins. Since the individuality of the worms is not accounted for in our model, $\boldsymbol{\sigma}^2_I$ represents the maximum potentially explainable variance in the data. The stereotypy-based model would be nearly perfect if $\boldsymbol{\sigma}^2_I$ were to drop to zero after the f^{-1} rescaling. To explore this, we plot the total variance of the active response $\boldsymbol{\sigma}^2_{\text{total}}$ (Fig. 2.5A), and the fraction

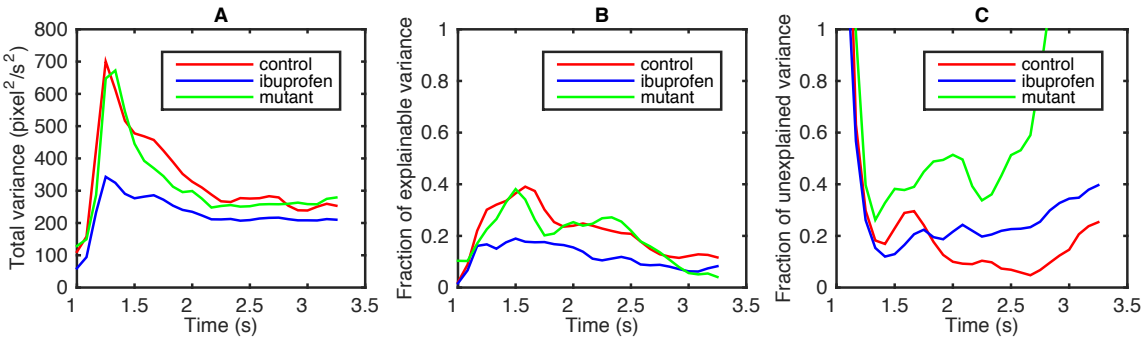

Figure 2.5: Variability of the active response. For the three worm types, in (A) we plot the total variance of velocity profiles $\boldsymbol{\sigma}^2_{\text{total}}$. Note that these numbers depend strongly on the preprocessing of the data – in particular, smoothing of the velocity (with the 500 ms filter, *Materials and Methods*) decreases the total variance. In (B) we show the fraction of potentially explainable variance $\boldsymbol{\sigma}^2_I/\boldsymbol{\sigma}^2_{\text{total}}$. Finally, (C) shows the part of the explainable variance that was not explained by our statistical model $\boldsymbol{\sigma}^2_{\text{res}}/\boldsymbol{\sigma}^2_I$. See the main text for the discussion of the differences between the three worm types on this plot.

of the potentially explainable variance, $\boldsymbol{\sigma}^2_I/\boldsymbol{\sigma}^2_{\text{total}}$ (Fig. 2.5B). The latter varies from 20% to 40% of the total variance, depending on the time post-stimulus and on the treatment. In both panels, the mutant and the control dataset are nearly indistinguishable, while the ibuprofen worms show a smaller variance, and a smaller fraction of the explainable variance. This is consistent with a smaller stimulus-driven response for this analgesic-like treatment.At the same time, these figures suggest that the decrease in the maximum reverse speed in the mutant worm (Fig. 2.2A) should not be attributed entirely to the reduced perceived heat stimuli. Indeed, the similarity of the variance and the explainable variance in the control and the mutant worms, which have very different mean maximum reverse velocities, suggests the existence of an additional (explainable, non-templated) component in the response behavior of the mutant, which is not present in the control.

The explainable variance $\boldsymbol{\sigma}^2_I$ is further split into the variance explained by the model, $\boldsymbol{\sigma}^2_{\text{m}}$, and the residual variance, $\boldsymbol{\sigma}^2_{\text{res}}$, which the model fails to explain:

$$\boldsymbol{\sigma}^2_I = \boldsymbol{\sigma}^2_m + \boldsymbol{\sigma}^2_{\text{res}}. \tag{2.11}$$

In Fig. 2.5C, we plot $\boldsymbol{\sigma}^2_{\text{res}}/\boldsymbol{\sigma}^2_I$, which is the fraction of the variance not captured by our model. Of the explainable variance, about 80% is captured by our model for the control and the ibuprofen worms in the window between 1 s and 3.3 s since the start of the trial, on average. This is a relatively large fraction for behavioral data, and provides an additional validation for our choice of a stereotypy-based model for representing escape behavior in these worms. Stability of the template itself between these two conditions, and the stability of the fraction of the explained variance suggest that much of the effect of ibuprofen can be attributed to the scaling of the templated response (and also the fraction of active worms). In other words, ibuprofen decreases the sensed heat stimuli.

In contrast, the unexplained variance for the mutant is about twice as large as that for the control, and approaches 100% at $t > 2.7$ s. This again illustrates that the templated response model is not very good for this treatment. Thus the mutations introduce changes in the behavior that are not consistent with a simple rescaling – mutations affect the fine motor behavior in addition to sensory system per se.

2.2.3 Using the statistical model

One of the goals of our study is to develop methods for quantitative assessment of the efficacy of pharmacological interventions to decreases sensed heat stimuli, at least in those cases where their action can be specifically interpreted as a change in thermal sensory transduction. We can use the developed statistical model for this. Specifically, taking the model derived from the control worms, we can infer the laser current from behavior of all three different worm types. To the extent that the current inferred for the treated worms is smaller than that for the control worms at the same applied current, the heat stimuli level perceived by the treated worms is smaller.

Figure 2.6 shows the overall structure of the inference done with the model. In the first row, we plot the conditional distribution of the inferred laser current given

the actual applied current I for the three worm types, $P(I_{\rm inf}|I, \text{type})$. We again bin the trials using I_i into five bins I_μ, $\mu = 1, \ldots, 5$ as before, and plot

$$P(I_{\rm inf}|I_\mu, \text{type}) = \sum_i^{N_{\rm type}} P_{\rm control}(I_{\rm inf}|\mathbf{v}_i) P_{\rm type}(\mathbf{v}_i|I_\mu). \tag{2.12}$$

Here $P_{\rm type}(\mathbf{v}_i|I_\mu)$ is 1 if the stimulus on the i'th trial for this worm type was in the I_μ bin, and zero otherwise. Further, $P_{\rm control}(I_{\rm inf}|\mathbf{v}_i)$ is given by the full model, Eq. (2.8), with the parameters inferred for the control worm, and with the empirically observed velocities $\mathbf{v}$ in trial i for each worm type. We see that there is more probability concentrated at small $I_{\rm inf}$ for the ibuprofen and the mutant worms, suggesting a reduction in the perceived stimulus level. Similarly, in the second row in Fig. 2.6, we plot the expected value, $\bar{I}_i$, of the distribution of the current inferred using the control model, $P_{\rm control}(I_{\rm inf}|\mathbf{v}_i)$, for each of the individual trials in each of the three worm types. To the extent that the values for the ibuprofen and the mutant worms are again somewhat lower than for the control worms, there is some reduction in the perceived current by this measure as well.

However, these population averaged results wash out important differences in the structure of the stimulus-response relationship. To quantify these small effects more accurately, we now look at the perceived stimulus changes for individual worms in the datasets. Specifically, for each trial i in the control dataset, a trial $j(i)$ with the closest value of the applied laser current is found in the ibuprofen / mutant dataset (the mean magnitude of the current mismatch is < 1 mA for both the ibuprofen and the mutant worms). We then use the control model to calculate the expected value of the inferred current for the jth trial in the ibuprofen / mutant datasets. This expectation is subtracted from the expectation value of the inferred current for the matched trial i for the control dataset. The difference of the expectation values, averaged over all control worms, is our measure of the reduction in the perceived

stimulus level

$$\Delta I_{\text{type}} = \frac{1}{N_{\text{control}}} \sum_{i}^{N_{\text{control}}} \left(I_{i,\text{control}} - I_{j(i),\text{type}} \right). \tag{2.13}$$

We evaluate ΔI_{type} for different worm types and for control worms binned into the five usual current bins (Fig. 2.7). To estimate the error of ΔI_{type}, we bootstrap the whole analysis pipeline, see *Materials and Methods*. There is a statistically significant difference in stimulus perception between the ibuprofen and the control worms. The difference is most significant when the actual laser current is around 100-110 mA. This coincide with our observation (Fig. 2.2A) that the most sensitive region of maximum reverse speed is around 100mA. Indeed, at smaller currents, the perceived stimulus level is small, many worms pause, and the behavior cannot be used to reliably estimate the stimulus level. At high current, the heat perception saturates, and all worms behave similarly, again reducing the ability to disambiguate the applied current level.

This analysis of ibuprofen worms achieves one of our main goals. It proves our ability to reconstruct stimulus from the behavior, and shows that analgesic-like effects of pharmacological perturbations can be quantified from the behavior. At the same time, ΔI_{mutant} turns out to be insignificant (Fig. 2.7B), even though a large statistically significant difference exists between the mutant and the control behaviors (Fig. 2.2A). This failure to detect a significant perceived stimulus reduction is because the templated response model is not very good for the mutant worm; thus our analysis cannot reliably assign a mutant trajectory on a given trial to a specific stimulus level. In other words, the large error bars in Fig. 2.7B serve as yet another check for self consistency: effects of the mutations cannot be attributed just to changes in stimulus perception.

2.3 Designing experiments: how many worms?

We expect our analysis to be useable for screening large numbers of chemicals for analgesic-like action. Since our approach targets one individual worm at a time, we

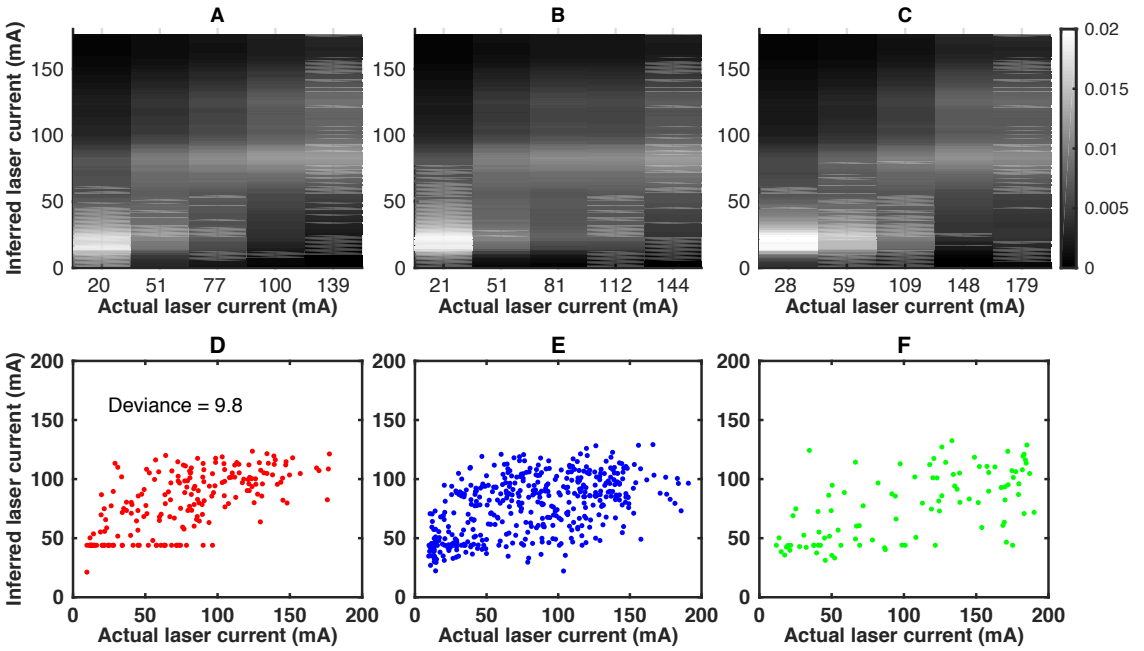

Figure 2.6: Inferring the perceived stimulus level from *C. elegans* escape behavior. The first row shows the conditional distributions of the inferred current vs. the actual applied current, partitioned into five bins, $P_{\text{control}}(I_{\text{inf}}|I_{\mu})$. Inference is done with the model of the control worm behavior. Panels (A), (B), (C) show the averaged probability of inferred laser current for the control, ibuprofen, and mutant worms, respectively. The second row shows the expected inferred laser current for each trial, $\bar{I}_{\text{inf},i} = \sum I_{\text{inf},i} P(I_{\text{inf},i}|\mathbf{v}_i)$ vs. the applied current I_i. The inference is again done using the control model, and panels (D), (E), (F) show the three worm types. The panel (D), (E), (F) is different from (A), (B), (C) since the first three show the average probability of inferred laser current while last three show the individual expected value of inferred laser current.

need to estimate the number of worms needed to achieve statistical significance in such screening experiments. For this, we fix the number of control worms, arguing that these must be only analyzed once, and hence a relatively large number of them can be tested. We then focus on ibuprofen, whose action is analgesic-like in our experiments, and on the bin at 110 mA, where the worms experience the most significant perceived stimulus reduction. There are $N_{\text{ibuprofen},110} = 94$ worms in this bin. We randomly sample with replacements $n < N_{\text{ibuprofen},110}$ worms from among these ibuprofen-treated worms and repeat our analysis pipeline, estimating the $\Delta I_{\text{ibuprofen}}(n)$. Resampling 1000 times (both the ibuprofen and the control datasets), we also estimate the vari-

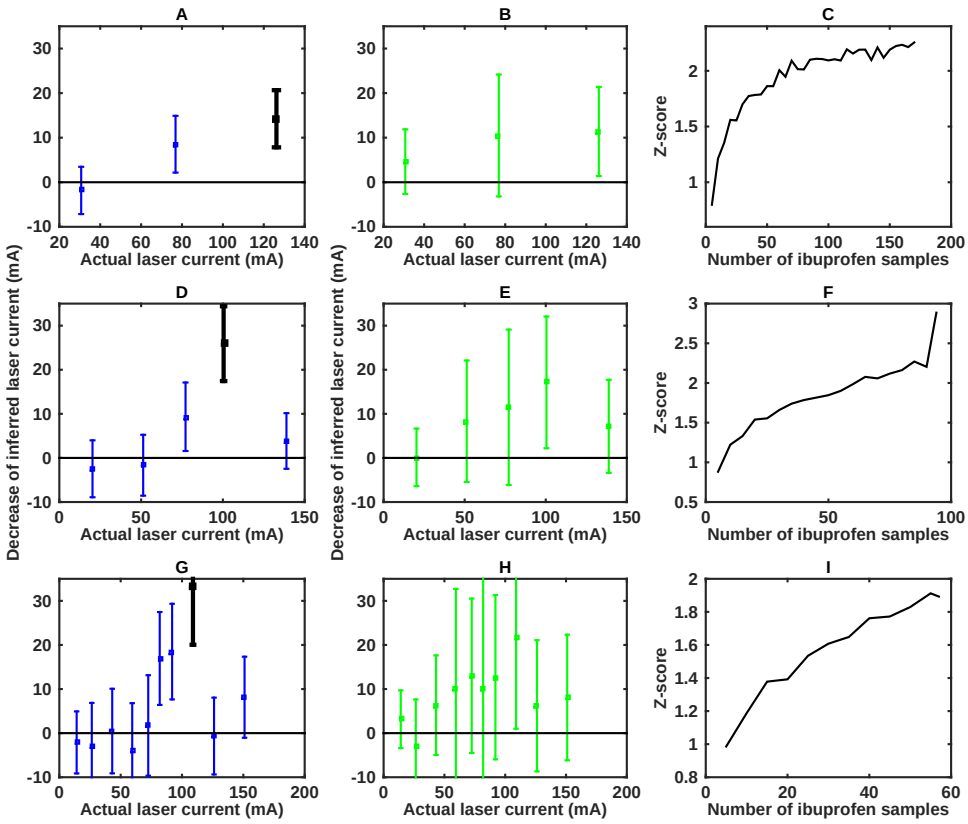

Figure 2.7: Perceived stimulus level decrease due to treatments. (A) Differences of the inferred laser current between the control and the ibuprofen datasets, $\Delta I_{\text{ibuprofen}}$. Errors represent standard deviations, estimated with bootstrapping. (B) Similar differences for the mutant worm, ΔI_{mutant}. Error bars are estimated by bootstrapping. (C) Dependence of the statistical significance of the perceived stimulus level reduction (measured by the Z score) for ibuprofen at 110 mA on the number of ibuprofen trials.

ance of $\Delta I_{\text{ibuprofen}}(n)$, and hence the Z score as a function of n (Fig. 2.7C). The plot here is an *underestimate* of the true Z score since resampling with replacements removes some stimulus values from the dataset, hence increasing the mismatch between control worms and the paired treated worms. Even with this, $Z \approx 2$ is achieved at $n \approx 60$ ibuprofen worms. In other words, in a typical screening experiment, one would need to test 200 or more worms to build the control model, and then at least ~ 60 worms additionally for each treatment condition.

2.4 Discussion

Typically a goal of sensory-response experiments is to develop a model that can predict the behavior in response to the stimuli. Here we wanted to do this in reverse. Our *grand goal* was to build a statistical model of the heat stimulus from careful measurements of the escape behavior of *C. elegans*, and to use this model to infer the changes in the perceived level of the stimulus felt by the organism due to perturbation in the sensory transduction pathway. Given this model, we could then measure changes in stimulus perception due to effects of chemicals and mutations, and use this as a basis to study the mechanism of sensory transduction in a genetically tractable organism amenable to high-throughput screens. As a representative data set, we choose to study the standard laboratory *C. elegans* strain N2, N2 treated with ibuprofen, and a mutant with defects in TRPV function. Other chemicals are also studied, but only ibuprofen is selected due to two reason. First, we selected chemicals that did not affect normal motion without laser stimulus, to make it more likely that the stereotypical behavior was not affected. Second, we made sure that the worm nonetheless displayed visually different behavior after the laser stimulus compared to N2 strain. Only ibuprofen passed these tests.

For the model to be successful, we had to meet a number of challenges. Since the worm could not communicate its perceived stimulus level to us directly we had to infer this level by reading the "body language" of the worm's escape response. The difficulty with quantifying a behavioral response as a measure of perceived stimulus level is that drugs or mutations can affect locomotory behavior in addition to perturbing sensory transduction. So in an attempt to deconvolve these effects, we used the entire behavioral profile instead of making ad hoc measurements. We leveraged the fact that escape responses in *C. elegans* turn out to be highly stereotyped, so that the escape response can be modeled with a velocity profile template that scales non-linearly in response to an applied laser current. The success of the template in modeling the

stereotyped wild-type escape response was confirmed by a functional collapse of the velocity profiles across different perceived stimulus levels. This discovery of invariance is important since it not only allowed us to effectively correlate escape behavior to the stimulus level, but it also allowed us to determine if the locomotory changes in our assay were due to changes specifically in the sensory transduction pathway or due to other general locomotory factors. By carefully accounting for the variation in our data and quantifying how much of this variation is captured by the model, we showed that the stereotypical behavior is unaffected by ibuprofen, save for changing the amplitude of the response. Thus this drug application likely reduced the perceived stimulus level in the worm. In contrast, a TRPV mutation changes locomotion in a way that is not as well captured by the template model. Thus we can be objectively critical about any inference made with this strain.

The model was also useful in determining key experimental parameters for future measurements. After verification that the model works well with the native and ibuprofen treated stimulus-response data, we quantified the changes in heat perception due to ibuprofen treatment. Our modeling and experimental assessment of escape behavior identified the optimal stimulus range and required number of trials to determine statistically significant differences between the inferred current of N2 in the untreated and treated conditions.

As a cautionary note, we point out that we avoid to call our heat stimulus as noxious, although the escape behavior of the worm in our experiment is similar to nociception. In the IASP definition, a nociceptive stimulus is an actually or potentially tissue-damaging event. The heat stimulus used in our experiment causes temperature increase of around 2°C in 0.1s, which does not have any evidence to damage the worm tissue. But previous research showed that the worm responses to small and rapid temperature increase in a nociception-like behavior [63]. Also a prolonged exposure to our heat stimulus is likely to cause damage to the worm tissue. Therefore

although we are not calling our stimulus as noxious, we believe our model will be valid for nociceptive behavior.

Also we point out that many noxious responses, especially in larger animals, are not stereotyped (and hence less studied), and not all stereotyped behaviors are noxious responses. The stereotypy of escape in *C. elegans* has turned out to be helpful in disambiguating qualitatively different effects that ibuprofen and mutations have on nociception, and it is likely to be equally helpful in the future in characterizing effects of other mutations and perturbations. However, by itself the stereotypy should not be viewed as evidence for a nociceptive response, and neither should the absence of stereotypy be used as an evidence that a response is not noxious.

In conclusion, we have solved what we defined as a grand problem in stimulus-response quantification and built a general model that connects stereotyped behavior to stimulus in the context of *C. elegans* heat-induced escape responce. With a language to describe this relationship, it is now possible to study quantitatively the effects of genetics and chemicals on this sensorimotor behavior. We believe that the utility of the model is quite general and could be applied to different model systems. However, we particularly hope that this work helps further establish *C. elegans* as a model for nociceptive research.

2.5 Materials and Methods

2.5.1 Worm preparation and experiment design

All worms were grown and maintained under standard conditions [75], incubated with food at 20 °C. Well fed worms were washed twice then gently spun down for 1 minute and the supernatant discarded by aspiration. We discovered empirically that ibuprofen affects the heat-induced escape response in our assay. For the drug application 100 μL of ibuprofen in M9 at 100 μM was added to the eppendorf tube. For the wild-type and mutant data set, M9 was used instead of the drug solution. Worms

were then placed in an incubator for 30 minutes at 20°C. After that worms were poured onto a seeded agar plate and transferred to agar assay plates by a platinum wire pick. These assay plates were incubated at 20°C for 30 minutes, and then the experimental trials were done within the next 30 minutes. In total $N = 201$ worms for the control group, $N = 441$ worms for the ibuprofen group, and $N = 100$ worms for the mutant group (ocr-2(ak47) osm-9(ky10) IV; ocr-1(ak46)) group were tested. The mutant strain was obtained from the Caenorhabditis Genetics Center.

The heat stimulation instrument has been described previously [63]. In summary, an infrared laser is directed to heat the head of a freely crawling worm ($\sim$ 0.5mm FWHM) on an agar plate. The laser pulse is generated with a randomly chosen laser current between 0 to 200 mA, with a duration of 0.1 s. The heating of the worm is nearly instantaneous, and it is directly proportional to the current, between 0 and 2 °C for the current range used in our experiments. The temperature change at 60 mA current is 0.4°C $\pm$ 0.03°C, 100 mA current is 0.89°C $\pm$ 0.05°C and 150mA current is 1.4°C $\pm$ 0.2°C. Worms were stimulated only once and not reused. The movements of the worms are imaged using a standard stereomicroscope with video capture and laser control software written in LabVIEW. For each stimulus trial, a random worm is selected on the plate and its motion is sampled at 60 Hz for 15 s, and the laser is engaged 1 s after the start of the video recording.

2.5.2 Data Analysis

The recorded response videos were then processed with Matlab to calculate the time series of the worm centroid motion as described previously [63]. All the worms that were not stimulated near the head or were not moving forward in the beginning of the video were discarded. Numerical derivatives of the centroid times series were then taken and filtered with a custom 500 ms Gaussian filter, which was a one-sided Gaussian at the edges of the recorded time period, becoming a symmetric Gaussian

away from the edges. This removed the noise due to numerical differentiation and also averaged out the spurious fluctuations in the forward velocity due to the imperfect sinusoidal shapes of the moving worm. We verified that different choices of the filter duration had little effect on the subsequent analysis pipeline. The direction of the velocity was determined by projecting the derivative of the centroid time series onto the head-to-tail vector for each worm, with the positive and negative velocity values denoting forward / backward motion, respectively.

The filtered velocity profiles needed to be subsampled additionally. This was because the statistical model of the data, Eq. (2.8), involved covariance matrices of the active and paused velocity profiles, Σ_p and Σ_a (note that velocity profiles are not temporally translationally invariant due to the presence of the stimulus, thus the full covariance matrix is needed, and not a simpler correlation function). To have a full rank covariance matrix, the number of trials must be larger than the number of time points. Alternatively, regularization is needed for covariance calculation. The autocorrelation function for all three worm types showed a natural correlation time scale of $\gtrsim 0.2$ s, whether the data was pre-filtered or not. Thus subsampling at a frequency > 5 Hz would not result in data loss. Therefore, instead of an arbitrary regularization, we chose to subsample the data at 12 Hz, leaving us with 37 data points to characterize the first 3 s of the worm velocity trace after the stimulus application, $1 \leq t \leq 4$ s since the start of the trial. Equation (2.8) additionally needs knowledge of T, the number of effectively independent velocity measurements in the profile. This is obtained by dividing the duration of the profile by the velocity correlation time. An uncertainty of such procedure has a minimal effect on the model of the experiment since it simply changes log likelihoods of models by the same factor, not changing which model has the maximum likelihood.

We then considered limiting the duration of the velocity profile used in model building: if velocities at certain time points do not contribute to identification of

I, they should be removed to decrease the number of unknowns in the model that must be determined from data (values of the templates at different time points). The first candidate for removal was the period of about 10 frames (0.16 s) after the laser stimulation since worms do not respond to the stimulus so quickly. However, removal of this time period had a negligible effect on the model performance, and we chose to leave it intact. In contrast, starting from 3.3 s (2.3 s after the stimulus) the fraction of explainable variance drops to nearly zero (Fig. 2.5) since many worms already had turned by this time and resumed forward motion. Therefore, we eventually settled on the time in the $1.0 \ldots 3.3$ s range for building the model.

Whenever needed, we estimated the variance of our predictions by bootstrapping the whole analysis pipeline [76]. For this, we created 1000 different datasets by resampling with replacement from the original control dataset and the mutant / ibuprofen datasets. Control statistical models (the scaling function f and the velocity templates) were estimated for each resampled control dataset. Standard deviations of these models were used as estimates of error bars in Fig. 2.4. For Fig. 2.7, we additionally needed to form the closest control / treatment worm pairs. These were formed between the *resampled* data sets for all worm types as well. Standard deviations of ΔI_{type} evaluated by such resampling were then plotted in Fig. 2.7 and used to estimate Z scores. Note that such resampling produces control / treatment paired worms that have slightly larger current differences than in the actual data; this leads to our error bars being *overestimates*.

Model in Eq. (2.1) requires knowing $P(I)$. In principle, this is controlled by the experimentalist, and thus should be known. In our experiments, $P(I)$ was set to be uniform. However, as described above, some of the worms were discarded in preprocessing, and this resulted in non-uniformly distributed current samples. To account for this, we used the empirical $P_{\text{emp}}(I)$ in our analysis instead of $P(I) = \text{const}$. In turn, $P_{\text{emp}}(I)$ was inferred using a well-established algorithm for estimation of one-

dimensional continuous probability distributions from data [77].

All of this analysis was implemented using Matlab, and the code is available for download from a public GitHub repository https://github.com/EmoryUniversityTheoreticalBi C.-elegans.

2.5.3 Calculating the template velocities, the covariances, and the scaling function

The template for the paused state $\mathbf{u}_p$ is calculated by taking the average of all paused velocity profiles for each of the three worm datasets. The covariance Σ_p is then the covariance of the set of the paused velocity profiles.

For active worms, we start with fixed putative parameter values $\mathcal{I}_1$ and $\mathcal{I}_2$. We then calculate the active template $\mathbf{u}_a$ and the covariance matrix $\sum_a$ by maximizing the likelihood in Eq. (2.7)

$$\frac{\partial \sum_i^{N_{\text{type},a}} \log P(\mathbf{v}_i|a, I_i)}{\partial \mathbf{u}_a} \propto \sum_i^{N_{\text{type},a}} \left[\mathbf{v}_i f_{\mathcal{I}_1,\mathcal{I}_2}(I_i) - \mathbf{u}_a f^2_{\mathcal{I}_1\mathcal{I}_2}(I_i)\right] = 0, \tag{2.14}$$

$$\frac{\partial \sum_i^{N_{\text{type},a}} \log P(\mathbf{v}_i|a, I_i)}{\partial \Sigma_a} \propto \sum_i^{N_{\text{type},a}} \left[\mathbf{v}_i - \mathbf{u}_a f_{\mathcal{I}_1,\mathcal{I}_2}(I_i)\right]^2 - (\Sigma_a)^{-1} = 0, \tag{2.15}$$

where $N_{\text{type},a}$ is the number of active worms of the analyzed type. This gives:

$$\mathbf{u}_a(\mathcal{I}_1, \mathcal{I}_2) = \frac{\sum_{i=1}^{N_{\text{type},a}} \mathbf{v}_i f_{\mathcal{I}_1,\mathcal{I}_2}(I_i)}{\sum_{i=1}^{N_{\text{type},a}} f^2_{\mathcal{I}_1,\mathcal{I}_2}(I_i)}, \tag{2.16}$$

$$\Sigma_a = \sum_i^{N_{\text{type},a}} \left[\mathbf{v}_i - \mathbf{u}_a f_{\mathcal{I}_1,\mathcal{I}_2}(I_i)\right]^2. \tag{2.17}$$

Having thus estimated $\mathbf{u}_a$ and Σ_a at fixed parameter values $\mathcal{I}_1$, $\mathcal{I}_2$, we maximize $\prod_i P(\mathbf{v}_i|a, I_i)$ over the parameters using standard optimization algorithms provided by MATLAB. We perform optimization from ten different initial conditions to increase the possibility that we find a global, rather than the local maximum.

Chapter 3 Cost of transport, not stability, predicts the walking speed distribution of *Drosophila melanogaster* at different ages

3.1 Introduction

Aging is associated with a myriad of behavioral changes [22, 28, 78, 79]. Perhaps the most studied age-related behavioral change is the reduction of locomotion speed, which is extensively studied in humans [80] and other animals [81, 25]. There are two hypotheses of this phenomenon: decrease in energy budget and decrease in motor control ability. Changes in energy budget during aging has been extensively studied [28, 82]. Studies in mammalian tissues [83] showed that aged tissues have reduced capacity to produce ATP, thus potentially reducing the energy sources for locomotion. Another possible explanation for age-related locomotion decline is motor control ability. Different studies have already hinted this may be a major factor. First, postural stability is one of the focus in aging research. Studies showed that human postural stability decreases with age [84, 85, 86]. To compensate the reduction of postural stability, aged human adopt a more conservative gait pattern, which reduces walking velocity [87]. Moreover, proprioception of humans and animals declines during aging [88, 89]. For fruit flies, proprioception deficiencies by mutation affect walking speed [90]. Missing, however, is an understanding of the relative contribution of these two factors to an animal's locomotion tendencies. In this paper, we study this relationship using the fruit fly *Drosophila melanogaster* as a model organism.

The fruit fly is one of the principal model organisms used for studying the effects of aging [22]. Many behavioral studies of aging have been conducted on the fly, including cardiac function [91], olfaction [26], stress resistance [92] and exploratory activity [25].

Such studies led to several important discoveries regarding genetics and environmental factors that influence life span [93, 94, 95]. They are suited for aging studies for several reasons. They develop to adulthood quickly and have a relatively short lifespan compare to mammalian models. They are easy and inexpensive to maintain, and many genetic tools are available. Furthermore, the fly is already established as a model for investigating age-related functional decline. Freely moving flies was shown to have less spontaneous locomotor activity when aged. [96].

To study the energy cost and stability of locomotion, we must first characterize the locomotion behavior of the fly comprehensively and quantitatively. In the last decade, many techniques have been developed to study the details of fruit fly locomotion. High temporal and spatial resolution tracking of each leg of a fly was designed for constrained spontaneous movement on a trackball [97]. For unconstrained locomotion, an automated system was developed to track and analyze the trajectory of multiple flies simultaneously [98]. In this project, we are utilizing a technique that allows high temporal and spatial resolution analysis of a freely moving fly [32]. This method captures high-resolution video of a fly moving in an arena, extracts the dynamics of its posture and classifies the animal's action into different behavioral modes. Our analysis on stability and energetic cost of locomotion is based on the postural dynamics from this method.

There have been many studies that aimed to investigate the motor control ability, or in other words the stability of locomotion, of legged animals. Most of these methods involved either a static measurement of center of mass [99] or a biomechanical model of locomotion [100, 101]. Very few of these studies tried to infer the stability from the postural dynamics data. In 1999, Full and Koditschek presented the *Templates and Anchors Hypothesis*, which suggested that locomotion can be modeled in two ways [102]. *Template* is a simplified model which serve as a guide for control of the body, while *Anchor* is a more biologically detailed model which allows

the template model to be embedded. This hypothesis suggests that in the high dimensional dynamics of animal locomotion, there exists a low dimensional attracting invariant manifold[36]. Base on this theory, Revzen and Guckenheimer [36] developed a method to reconstruct the dynamics of systems with a limit cycle from time-series data. This approach utilizes the Floquet theory to estimate how fast does the system recover from perturbations away from the limit cycle. This method gives us a measurement of stability by the estimating the time scale of perturbation recovery during locomotion.

Several methods have been developed to estimate energy expenditure of locomotion. One way is to measure index of metabolic rate such as oxygen consumption [103] and external load [103]. The other method is to estimate the energy consumption through a biomechanical model of leg dynamics. Nishii [33, 34] proposed an analytical estimation of energy cost (cost of transport) legged movement by modeling the leg as links and joints. In this model, the cost of transport is given by the sum of mechanical work and energy dissipation. The physical parameters of the model are quantified by high-speed imaging [90],[104].

In this paper, we study the relationship between speed distribution, energy cost of transport and stability. We estimate the cost of transport and measure gait stability of freely behaving flies of varying ages. Through building a linear regression model that predicts speed distribution from energy cost of transport and stability, we discover that the cost of transport, not stability, determines the speed distribution. Finally we discover that this relationship does not change with the age of the fly. This result suggests that the walking speed distribution is not limited by the motor control ability, but the energy budget of the fly.

3.2 Experiment

The experimental setup is the same as used in Berman et al. [32]. Here the spontaneous behavior of ground-based fruit flies (D. melanogaster) were studied in a featureless circular arena. The arena was constructed as a thin chamber with gently sloping sides to prevent flies from flying, jumping and climbing the walls. To prevent the flies from adhering to the ground, the underside of the arena was coated with repellent saline compound. The flies were recorded with sufficient spatial-temporal resolution (100Hz, 1088×1088 pixels) to resolve moving body parts such as legs. The camera was controlled by a LabView-based tracking system to keep to the fly inside the frame.

We studied the behavior of 275 male flies with an age of 1 to 71 days after eclosion. Each fly was isolated within 4 h of eclosion. Before the start of the recording, the flies were transfered to the arena via aspiration and allowed 5 minutes or adaptation. Then it was imaged for 1 hr, yielding 9.9×10^7 frames in total for all 275 flies. All of the recordings occurred between 9:00 and 13:00 in a temperature of 25 degree Celsius.

The data were then used to generate a two-dimensional behavioral map that separates stereotyped behavior using unsupervised approaches (for full details see [32]). The images were first segmented from the background, rescaled to a reference size and then aligned by their head-to-tail vector. Then a set of 50 basis vectors of flies' posture was generated using Principle Component Analysis (PCA). Time series were produced by projecting the pixels of the images onto the basis set. The spectrogram of these projections was then embedded into two dimensions using t-Distributed Stochastic Neighbor Embedding (t-SNE) [105]. Each point on the behavioral map represent a unique set of postural dynamics, and the nearby positions represent similar motion. This is due the fact that t-SNE algorithm preserves the local relationship when embedding the high dimensional data into a low dimensional map. The behavior of each region on the map was identified manually and the corresponding projection time

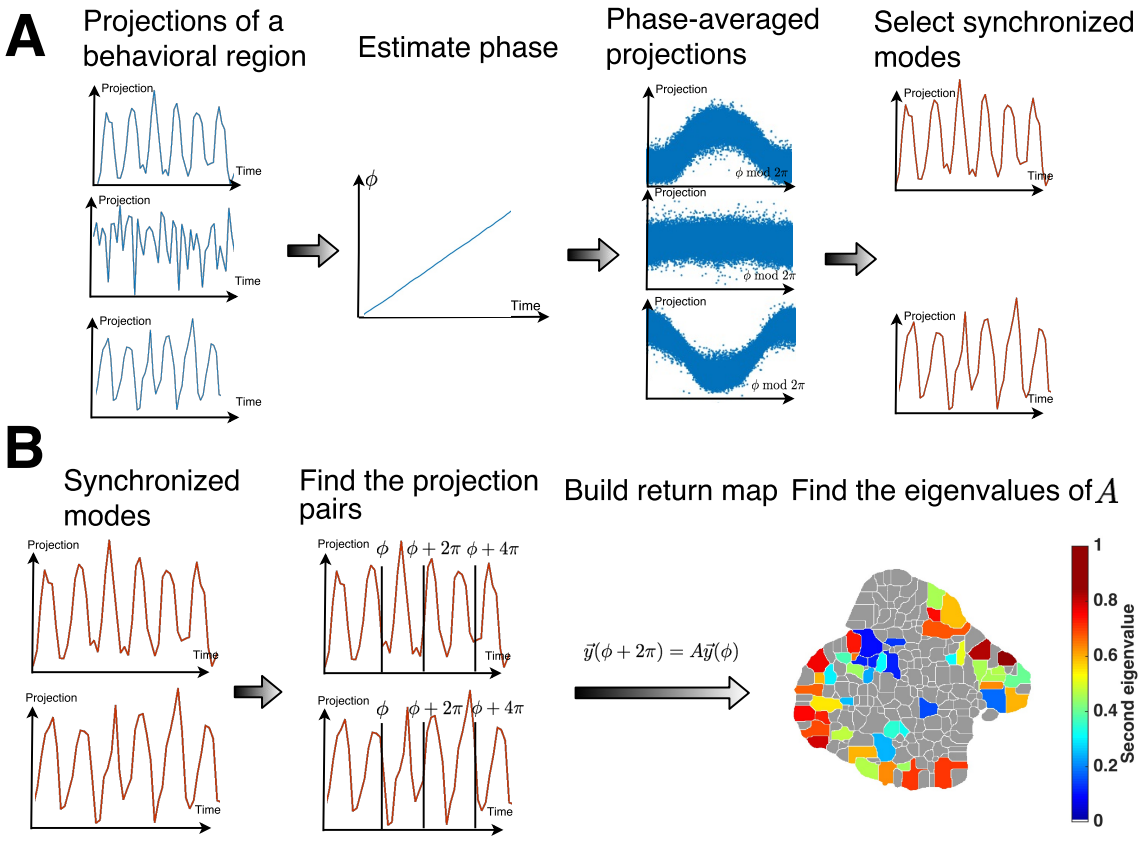

Figure 3.1: Data analysis pipeline overview. (a) For a specific behavioral region, the projections of different modes in this region are extracted and then estimated the phase value. The synchronization parameter of each mode is then calculated by phase-averaged projections. Then synchronized modes are defined by the modes that have a synchronization parameter larger than 0.5. (b) The projection pairs $y(\phi)$ and $y(\phi + 2\pi)$ are then selected for each of the synchronized modes. The return map is estimated by linear regression and the eigenvalues of the return map is computed.

series become the basis of our analysis.

3.3 Analysis

The analysis of fly behavior is composed of two sections. First, we determine the stability of a specific behavioral region using Floquet theory [36]. The stability is defined as the characteristic decay time of perturbation. Second, we estimate the power consumption of the behavior by an biomechanical model [33, 34]. The physical parameters of the model is obtained from previous research [106, 90].

3.3.1 Estimating stability by Floquet theory

The framework of stability analysis is described in figure 3.1. We use a modified algorithm based on Revzen & Guckenheimer [36], which is based on Floquet theory, to find out the stability of locomotion. Floquet theory states that for a linearly driven periodic system

$$\dot{y}(t) = A(t)y(t), \tag{3.1}$$

where $A(t)$ is periodic

$$A(t+T) = A(t), \tag{3.2}$$

the fundamental matrix solution ϕ has the form

$$\phi(t) = \sum_i Q_i(t)e^{tR_i}, \tag{3.3}$$

where $Q_i(t)$ are linearly independent and periodic, and the factor e^{tR_i} are called the Floquet multipliers. The Floquet multipliers determine how fast each mode decays with time. The Floquet multipliers are given by the eigenvalues of the return map A.

$$y(\phi+T) = Ay(\phi), \tag{3.4}$$

In our analysis, the periodic system is the postural dynamics of the fly. By Floquet theory, the solution can be mapped into a combination of periodic functions and the corresponding decay functions. The decay function represents the characteristic time of the corresponding component of the periodic postural dynamics. The longest characteristic time represent the main locomotion behavior of the fly. The second longest characteristic time represents the decay time of perturbation. Therefore we select the second longest characteristic time as a proxy for the stability of the fly behavior.

3.3.2 Stability analysis algorithm

The raw behavioral data $\vec{y}_i$ are the time series projections on 50 eigenmodes of the posture and the corresponding watershed behavioral region index. The locomotion

data is first isolated using the embedding method developed by Berman et al. [32]. At the each analysis cycle, we select a specific locomotion region and the corresponding projection data series. The separate data series are catenated together with the first 2 and last 2 frames (0.02 sec) discarded to avoid artifacts in phase estimation. Each series is subtracted by its mean over time before catenation. We then use the Phaser phase estimation algorithm developed by Revzen & Guckenheimer [35] to estimate the phase of the projection $\hat{\varphi}_i$.

Since not every eigenmode is synchronized with the dynamics, we use an iterative heuristic to select the synchronized modes. At each cycle we estimate the phase and calculate the synchronization parameter of each mode, which is defined as the ratio between explained variance by the phase and variance of projection of each mode. We then choose the modes for next cycle by a linearly increasing threshold. After 20 cycles and maximum threshold of 0.5, a set of synchronized modes are selected for each behavioral region. For some regions, none of the modes are synchronized and the region is not used in our analysis.

Then for each valid behavioral region, we extract the points on the Poincare section $\vec{y}_i$ at target phase $\phi_j = \phi_0 + 2\pi j$ by linearly interpolating between adjacent data points. Then we calculate the return map by multivariate regression on projection pairs $\vec{y}_i$ and $\vec{y}_{i+1}$. The Floquet multipliers are given by the eigenvalue of the return map matrix A. Contrary to deterministic noiseless dynamical systems, we expect the Floquet multipliers to vary between the Poincare section, as noted in human and cockroach data [107, 36]. To address this problem, we calculate the empirical distribution β_ϕ of the return map A_ϕ by bootstrapping the pairs $\{\vec{y}_i, \vec{y}_{i+1}\}$ while retaining the relationship between the points. The empirical distribution allow us to estimate the confidence level of the Floquet multipliers. Moreover, to select a proper Poincare section, we compute the multiplier for 100 equally spaced phases around the cycle and pick the phase value with largest multiplier closest to 1.

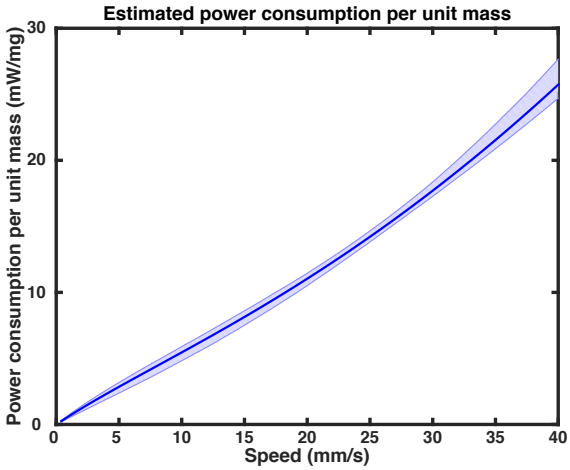

Figure 3.2: Power consumption per unit mass as a function of speed. The power consumption is estimated by the method mentioned in Nishii 2006. In this model we used the physical parameters estimated in Mendes et al. 2013.

3.3.3 Power consumption

The power consumption of locomotion is difficult to measure directly from experiment. Therefore we use an analytical estimation developed by Nishii [33, 34] to calculate the power consumption. In the model, there are two phases of locomotion: stance and swing. The stance phase represent the phase when the leg exert force on the ground and push the body forward. The swing phase represent the phase when the leg is moving forward to the starting position. In each phase there are two sources of energy consumption: mechanical work and heat dissipation. Combining these four factors, we estimate the power consumption per unit mass of fly as a function of speed (figure 3.2). The power consumption has a non-linear relationship with speed.

$$e(V, \beta, S) = e_w^{sw} + e_w^{st} + e_h^{sw} + e_h^{st} \tag{3.5}$$

Where e_w^{sw}, e_w^{st} represent the work done in swing and stance phase, and e_h^{sw}, e_h^{st} represent heat dissipation in swing and stance phase respectively. Their analytical form is shown as follows:

Table 3.1: Parameters of locomotion energy consumption model

Body weight M	0.25 mg [106]
Body length	2.5 mm [106]
Stance length S	$0.04711 \times V + 0.748$ [90]
Velocity V	0-30 mm/s [106]
Length of leg l	1.25 mm [106]
Moment of inertial of the leg I	0.0156 mgmm^2 [106]
Duty ratio β	$\frac{t_{st}}{t_{st}+t_{sw}}$
Stance duration t_{st}	$11.5 + (910/V)$ [90]
Swing duration t_{sw}	$(-0.126 \times V) + 36.56$ [90]

$$e_w^{sw} = \frac{nI}{l^2 M} \frac{\beta V^2}{S} \frac{1+\beta^2}{(1-\beta)^2} \tag{3.6}$$

$$e_w^{st} = \frac{1}{8l} S \tag{3.7}$$

$$e_h^{sw} = \gamma \frac{2n\pi^2 I^2}{l^2 M} \frac{V^3 \beta^2}{(1-\beta)^3 S^2} \tag{3.8}$$

$$e_h^{st} = \gamma \frac{M}{n} \frac{1}{\beta V} \left(\alpha^2 + \frac{S^2}{12}\right) \tag{3.9}$$

Where n is the number of legs, M is the body weight, S is stance length, V is locomotion speed, β is the duty ratio, l represent the length of a leg, I is the moment of inertia of the leg around its joint. These physical parameters are estimated from Isakov et al. and Mendes et al. [106, 90]. Values of the parameters and scaling relationship between duty ratio and speed are listed in Table 3.1. The stance length (step length) is estimated by a regression model from speed according to Mendes et al. [90]. The factor γ represent the ratio of heat dissipation to mechanical work and α is the amplitude of the torque required to maintain a bent leg posture. We are using the values from Nishii 2006 [34] for these factors.

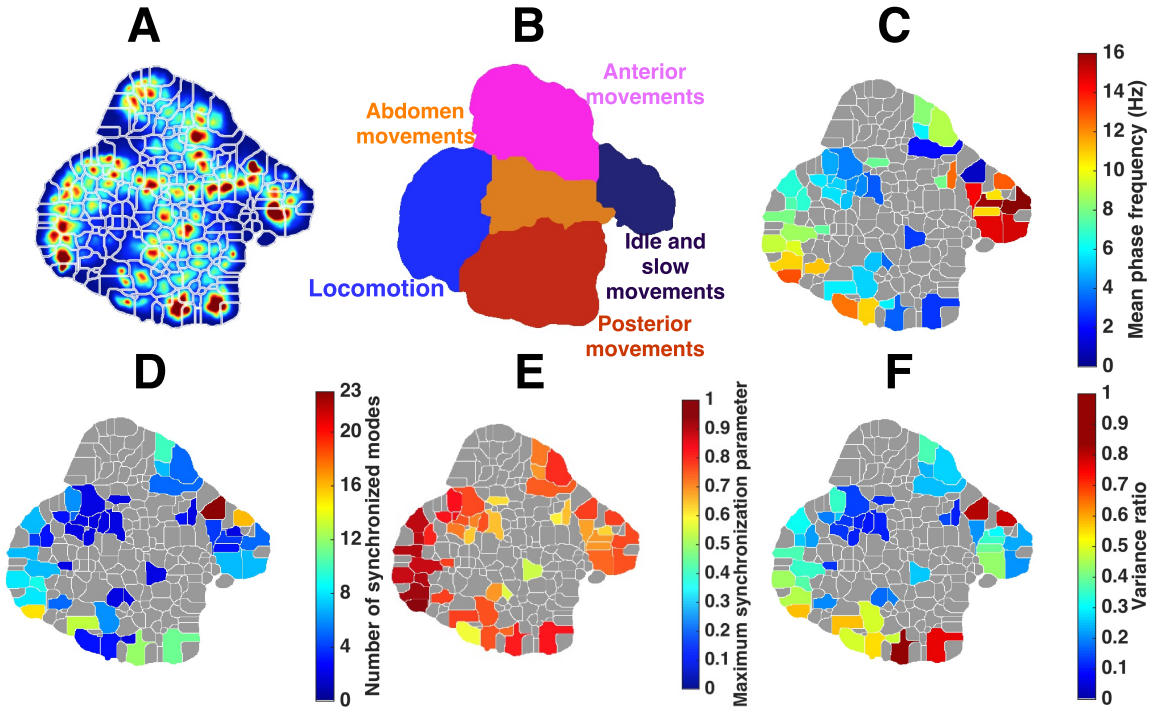

Figure 3.3: Statistics of analysis of different behavioral region. Grey color denote regions that do not have enough data to estimate the statistic. (a) Probability density function of behavior space and segmentation of behavioral region (b) Functional description of behavioral regions. The characterization of behavioral region is performed through visual assessment.(c) Mean phase frequency of estimated phase. (d) Number of synchronized modes. (e) Maximum synchronization parameter of each behavioral region. (f) Variance of synchronized modes as a ratio of total variance of all modes.

3.4 Results

3.4.1 Phase estimation and synchronization

Figure 3.3 shows the statistics of the phase estimation and synchronized modes. Similar to the results in Berman et al. [32], we notice that there are several different phase frequencies in the locomotion regions. The fastest region has a phase frequency at around 13Hz, which correspond to around 20 mm/s. For all the behavioral regions, the number of synchronized modes ranges from 0 to 23 (figure 3.3b). In the locomotion region, there are 8 to 15 synchronized modes. The maximum value of synchronization parameter of each behavioral region varies, but the values are higher in the locomotion

region compare to other region (figure 3.3c).

We quantify the statistical power of the synchronized modes by calculating the fraction of variance it explained. In the locomotion region, this number ranges from 0.3 to 0.6.

3.4.2 Stability at different behavioral region

To systematically investigate the relationship of locomotion speed and stability, we focus on several locomotion regions with the highest probability density function (figure 3.3e). For each behavioral region, we catenate all projection time series and estimate the absolute value of the Floquet multipliers (figure 3.4a). The largest multipliers in different locomotion regions have an absolute value near one, indicates the dominant components have a very large decay characteristic time. This is because in our analysis, we select the data of the animal performing a specific behavior. Therefore the corresponding periodic trajectories in the postural space should oscillate indefinitely, and the largest Floquet multiplier should be close to one.

Since the most stable component is the locomotion behavior itself, the second largest Floquet multiplier represents the decay time of perturbation. If the locomotion is stable, the decay characteristic time and the multiplier should be small. We estimate the multipliers at different behavioral regions (figure 3.4c) and discover that the stability decreases when the locomotion speed increases. Note that for some regions, there are not enough projection pairs to compute the multiplier.

3.4.3 Stability of different age groups

To understand the effect of age on the stability of locomotion, we divide the data into five groups, each representing a 14 days period. We analyze the data with the same method and project them onto the same behavioral map. But even in the same behavioral region, the animals behaves differently. In the fastest locomotion region, the average frequency of phase estimate decreases with time (figure 3.5a). Therefore

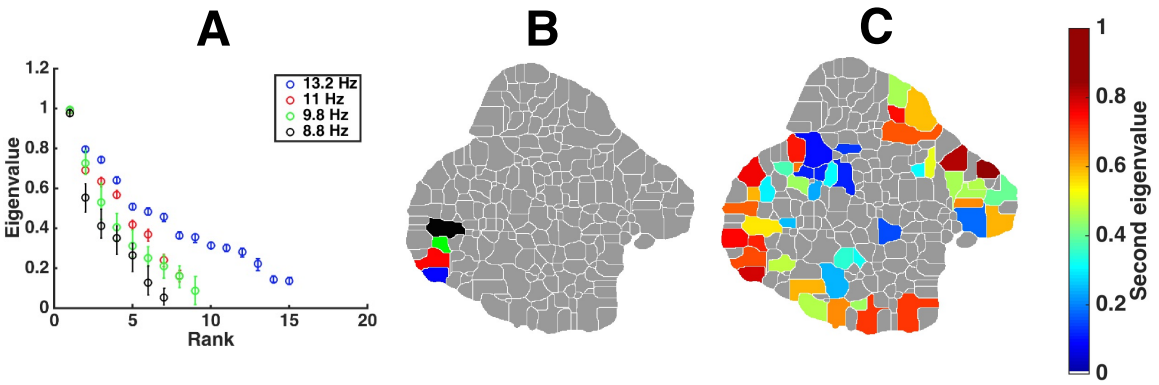

Figure 3.4: Eigenvalue rank plot of locomotion region. (a) The eigenvalues of four locomotion region with different speed. The errorbars are estimated by bootstrapping the projection pairs. (b) Region corresponding to (a), coded by color. (c) Map of second largest eigenvalues at different behavioral region. Grey area denote behavioral regions that do not have enough data to estimate the eigenvalues.

we convert the Floquet multipliers to a characteristic time to represent the dynamical stability of the specific behavior. The characteristic time is defined by

$$t^* = \frac{-1}{f \log M} \tag{3.10}$$

where M is the second largest Floquet multiplier and f is average frequency of the phase in the behavioral region. This is equivalent to the time need for the perturbation to decay to $1/e$ of the initial amplitude.

In general, the relationship of locomotion speed and stability is preserved during aging. The characteristic time of the fastest locomotion is the largest, suggesting the stability is the lowest. For most of the locomotion regions, the 15-28 days period has the highest stability, and then the stability decreases with age. This confirm with previous studies that stability of locomotion decreases with age.

3.4.4 Relationship between speed, stability and power consumption of different age groups

To understand to what extent a decrease in energy budget and ability to control motor system affect the reduction of locomotion speed, we use a linear regression

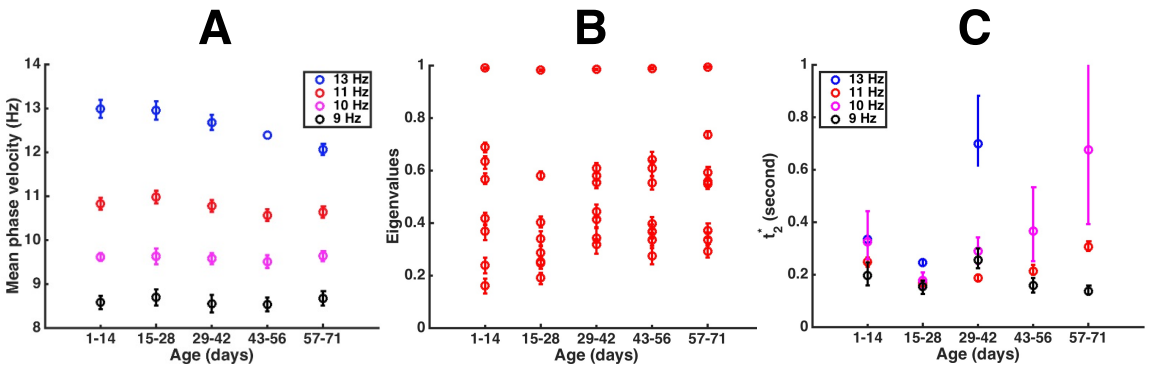

Figure 3.5: Behavioral dynamics. (a) The mean phase frequency of locomotion region as a function of age. (b) The eigenvalues of locomotion region with speed equal to 11Hz. (c) The characteristic time of perturbation of different locomotion region as a function of age. Note that for the 13Hz locomotion, there are not enough data to estimate the Floquet multipliers of older age groups.

model to estimate the relationship between probability of speed, stability and power consumption at different locomotion regions. Similar to previous section, we bin the data set into five different age groups and estimate the parameters separately. In the model, we represent stability by the characteristic time t^*. The relationship is shown as follows:

$$\log(P) = \beta_0 + \beta_1 \log(e) + \beta_2 t^* \tag{3.11}$$

where P represents the probability of speed. Figure 3.6a,b shows that power consumption is highly correlated with speed distribution while characteristic time (stability) does not exhibit any correlation. This observation is confirmed by the regression parameters. The parameters for power consumption are significantly smaller than zero, indicating a negative relationship between power consumption and speed distribution. The parameters for stability (t^*) are not significantly different from zero, indicating stability does not have a linear relationship with speed distribution.(Figure 3.6d, e, f) The scatter plot of probability of speed and stability further shows that it is highly unlikely that another nonlinear structure exists (Figure 3.6b). As a comparison, we also studied linear models with stability or log power consumption only. Table 3.2

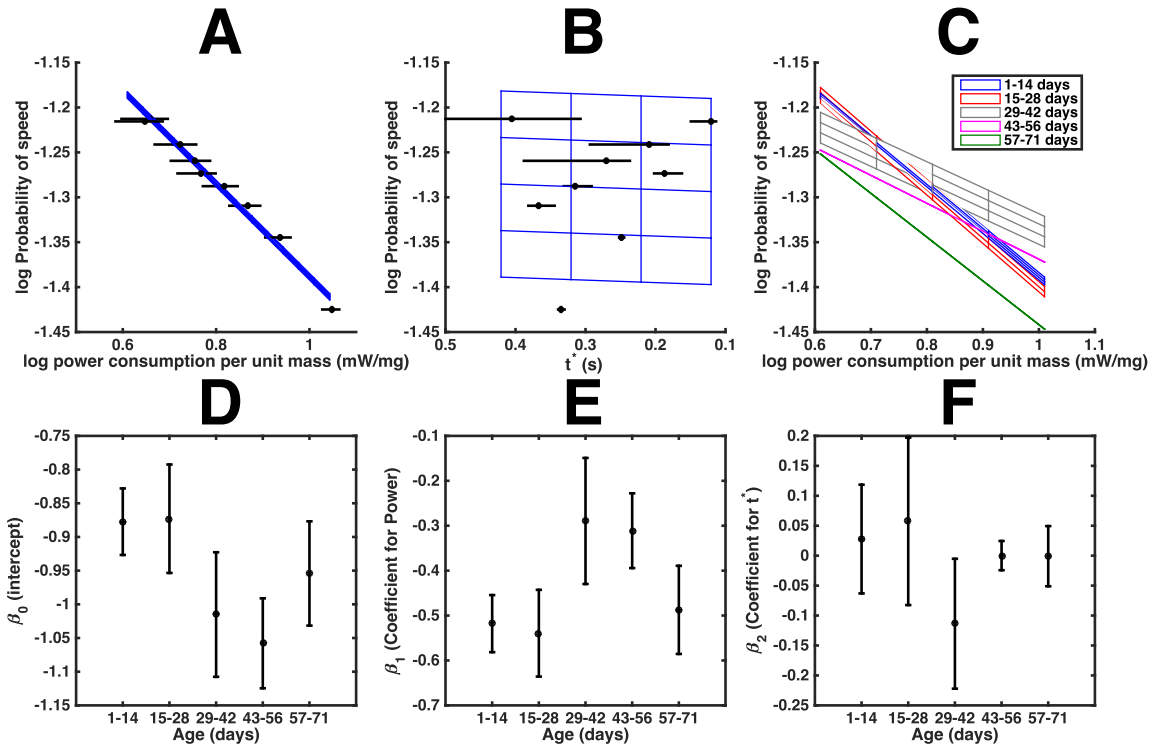

Figure 3.6: Relationship between probability of speed, stability and power consumption of different age groups. (a) Relationship between log probability of speed and log power consumption of flies in 1-14 days. The surface denote the regression model, and each data point represent a locomotion region. (b) Relationship between log probability of speed and stability measured in characteristic time of flies in 1-14 days. The surface denote the regression model, and each data point represent a locomotion region. (a) and (b) represent the same model in different perspective. (c) Relationship between log probability of speed and log power consumption of flies of different age groups. Each surface represent a regression model. (d) Regression model intercept of different age groups. (e) Regression model coefficient of power consumption. (f) Regression model coefficient of stability measured in characteristic time.

Table 3.2: BIC score of different relationship models at different ages

Model	1-14 days	15-28 days	29-42 days	43-56 days	57-71 days
stability only	-3.2	-0.5	-18.0	-14.2	-5.2
power consumption only	-43.2	-35.2	-31.4	-41.6	-32.4
stability and power consumption	-39.4	-29.7	-30.7	-35.8	-30.2

Table 3.3: R^2 of different relationship models at different ages

Model	1-14 days	15-28 days	29-42 days	43-56 days	57-71 days
stability only	0.09	0.002	0.73	0.03	0.01
power consumption only	0.98	0.97	0.92	0.97	0.96
stability and power consumption	0.99	0.97	0.95	0.95	0.98

and 3.3 present the Bayesian information criterion (BIC) score and R^2 of different models as a function of age. From Table 3.2, we note that the BIC score of power consumption only model is less than other models. Therefore we can conclude that power consumption is the major factor in determining the speed distribution of the fly.

Age of the fly changes the relationship between speed distribution, stability and power consumption, but stability still plays an insignificant role in the relationship in all age groups. The parameter of stability does not exhibit any significant difference when age changes (Figure 3.6f). At older (57-71 days) and younger age groups (1-14 and 15-28 days), the power consumption has a greater negative impact on speed distribution compare to middle age groups (29-42 and 43-56 days)(Figure 3.6e). This coincide with the observation that middle aged flies spend a significantly more time in faster locomotion, compare to older or younger flies. The intercept, which represent the baseline of the magnitude of speed distribution, also support this observation (Figure 3.6d).

3.5 Discussion

We design a method to determine the quantitative relationship between speed distribution, power consumption and stability. We estimate the stability of locomotion using Floquet theory from postural dynamics, and power consumption by a biomechanical model with physical parameters estimated from other studies. Locomotion behavior is identified by a map of behavior from postural data. Contrary to many observation and hypothesis [108, 109], we found that the stability of locomotion has no significant correlation with speed distribution. The power consumption has a much stronger predictive power to speed distribution. By building a regression model, we discovered that the power consumption has a strong linear relationship with the speed distribution.

Combine with tools of genetic and neural perturbation, we can now study quantitatively how different perturbation is affecting the stability and distribution of locomotion behavior. We stress that we do not present this result as a causal relation between speed distribution and power consumption. Our study suggest a strong correlation, but further studies are required to uncover the mechanism of the fly to determine its locomotion speed.

Finally, we note that this method is not limited to *Drosophilia* locomotion. The stability analysis algorithm is not dependent on any specific animal. Given that behavior is periodic and with sufficient data, this algorithm is able to analyze stability. On the other hand, the Energy consumption model can be generalized to any legged locomotion. This allows potential application to different animals and find out the relationship of speed distribution with stability and energy consumption.

Chapter 4 Summary and outlook

Animal sensorimotor behavior is an intriguing but complex phenomenon. While the underlying mechanisms are not clear in most cases, in this thesis I demonstrate that it is possible to infer a statistical relationship between sensory information and locomotion behavior. Since locomotion is highly stereotypical, high dimensional behavioral data can be reduced to low dimensional space [15, 32]. At the same time, the stereotypical behavior enables us to classify different behavioral modes of an animal. Through these properties, I develop two models for *C. elegans* and *D. melanogaster* using techniques from Bayesian inference and dynamical system theory. These approaches reveal important features that predict thermal noxious stimulus in worms and walking speed distribution in fruit flies.

The statistical model in Chapter 2 allows us to infer the strength of heat stimulus from the escape behavior of *C. elegans*, and to use this model to measure the changes in perceived level of stimulus felt by an individual animal due to the effects of chemicals and genetic mutation. Using the entire escape profile, instead of ad hoc measurements, this model can infer the posterior probability of perceived stimulus level. Moreover, by comparing the escape response profile to wild-type response template, we can distinguish changes to the sensory system and motor system. Most of the nociceptive assays in previous studies are not able to address this difference. In our case, the stereotypical escape behavior is not affected by ibuprofen, while TRPV mutation affects the stereotypical behavior significantly. Therefore, ibuprofen is likely to reduce the perceived pain level, while we cannot make any inference of analgesic effects of TRPV mutation. This method can be used to build a high-throughput experiment system to study the genetics of nociception or find out possible candidates for analgesics.

Besides *C. elegans*, many other animal models are used for nociception studies [110]. It is natural to develop statistical models or machine learning methods to infer the level of pain in other animals. One of the possible directions is inferring perceived pain of rodents. With a manual behavioral coding system, perceived pain level and effect of analgesics can be estimated [111] from facial expression. But similar to other assays, this method focuses on ad hoc components of behavior. It would be interesting to improve this process by using facial expression recognition techniques developed in computer vision [112] to build a nociception assay base on stereotypical behavior.

Besides inferring the sensory system input, I also investigated the possibility of inferring behavioral strategies through quantifying locomotion. In particular, I focus on the change of locomotion speed distribution during aging. There are two major hypothesis of reduction of walking speed - reduction of energy budget [28, 83, 113] and locomotion stability [108, 114, 109, 115]. In Chapter 3, I attempt to study this relationship by estimating the stability and energy budget during locomotion of freely walking fruit fly *D. melanogaster* at different ages. Through method developed from dynamical system theory [35, 36] and biomechanics [34, 33], I determine that energy cost of transport, not stability, predicts the walking speed distribution. This statistical relationship cannot explain the causal relationship between these factors, and further experiments are needed in this direction. For example, to validate the relationship between energy cost of transport and walking speed distribution, we can investigate the same relationship with different mass added to the freely walking fly. Furthermore, recent research discovered that the fly behavior exhibits multiple time scales and can be organized into a hierarchical structure [116]. It would be interesting to see how aging affects the transition of locomotion states and how locomotion stability and energy cost determine the distribution and transition of these locomotion states.

In summary, in this thesis, I demonstrated the possibility to infer characteristics of

sensorimotor behavior by quantifying dynamics of animal locomotion. These models help us to understand more about the behavioral strategies during aging, the relationship between nociception and escape behavior, and developing new analgesics in the future. I hope this will lay down the foundation for further research on animal behavior in the future.

Bibliography

[1] Michael F Frampton. "Aristotle's Cardiocentric Model of Animal Locomotion". In: *Journal of the History of Biology* 24.2 (1991), pp. 291–330.

[2] Sydney Brenner. "The genetics of Caenorhabditis elegans". In: *Genetics* 77.1 (1974), pp. 71–94.

[3] Theodore B Achacoso and William S Yamamoto. *AY's Neuroanatomy of C. elegans for Computation*. CRC Press, 1991.

[4] Donald L Riddle et al. *C. elegans II*. Cold Spring Harbor Laboratory Press, 1997.

[5] T Kaletta and M O Hengartner. "Finding function in novel targets: C. elegans as a model organism". In: *Nat Rev Drug Discov* 5.April (2006), pp. 387–398.

[6] Ann K. Corsi, Bruce Wightman, and Martin Chalfie. "A transparent window into biology: A primer on Caenorhabditis elegans". In: *WormBook*. Vol. 200. 2. The C. elegans Research Community, 2015, pp. 387–407.

[7] Eviatar Yemini et al. "A database of Caenorhabditis elegans behavioral phenotypes". In: *Nature methods* 10.9 (2013), pp. 877–879.

[8] J Hodgkin. "Male Phenotypes and Mating Efficiency in Caenorhabditis elegans." In: *Genetics* 103.1 (1983), pp. 43–64.

[9] Wei Geng et al. "Quantitative Classification and Natural Clustering of *Caenorhabditis elegans* Behavioral Phenotypes". In: *Genetics* 165.3 (2003), pp. 1117–1126.

[10] Joong Hwan Baek et al. "Using machine vision to analyze and classify Caenorhabditis elegans behavioral phenotypes quantitatively". In: *Journal of Neuroscience Methods* 118.1 (2002), pp. 9–21.

[11] Christopher J Cronin et al. "An automated system for measuring parameters of nematode sinusoidal movement". In: *BMC genetics* 6.1 (2005), p. 5.

[12] Katsunori Hoshi and Ryuzo Shingai. "Computer-driven automatic identification of locomotion states in Caenorhabditis elegans". In: *Journal of neuroscience methods* 157.2 (2006), pp. 355–363.

[13] Kuang-Man Huang, Pamela Cosman, and William R Schafer. "Machine vision based detection of omega bends and reversals in C. elegans". In: *Journal of neuroscience methods* 158.2 (2006), pp. 323–336.

[14] Nicolas Roussel et al. "A computational model for C. elegans locomotory behavior: application to multiworm tracking". In: *IEEE transactions on biomedical engineering* 54.10 (2007), pp. 1786–1797.

[15] GJ Stephens et al. “Dimensionality and dynamics in the behavior of *C. elegans*”. In: *PLoS Comp Biol* 4.4 (2008), e1000028.

[16] Greg J Stephens et al. “Emergence of long timescales and stereotyped behaviors in *Caenorhabditis elegans*.” In: *Proc Natl Acad Sci USA* 108.18 (2011), pp. 7286–7289.

[17] Edward M Hedgecock and Richard L Russell. “Normal and mutant thermotaxis in the nematode Caenorhabditis elegans”. In: *Proceedings of the National Academy of Sciences* 72.10 (1975), pp. 4061–4065.

[18] M Chalfie et al. “The neural circuit for touch sensitivity in *Caenorhabditis elegans*.” In: *J Neurosci* 5.4 (Apr. 1985), pp. 956–964.

[19] Cornelia I Bargmann. “Genetic and cellular analysis of behavior in C. elegans”. In: *Annual review of neuroscience* 16.1 (1993), pp. 47–71.

[20] Mario de Bono and Andres Villu Maricq. “Neuronal substrates of complex behaviors in C. elegans”. In: *Annu. Rev. Neurosci.* 28 (2005), pp. 451–501.

[21] Mark D Adams et al. “The genome sequence of Drosophila melanogaster”. In: *Science* 287.5461 (2000), pp. 2185–2195.

[22] Michael S Grotewiel et al. “Functional senescence in Drosophila melanogaster”. In: *Ageing research reviews* 4.3 (2005), pp. 372–397.

[23] Robert RH Anholt and Trudy FC Mackay. “Quantitative genetic analyses of complex behaviours in Drosophila”. In: *Nature Reviews Genetics* 5.11 (2004), pp. 838–849.

[24] Julia Warner Gargano et al. “Rapid iterative negative geotaxis (RING): a new method for assessing age-related locomotor decline in Drosophila”. In: *Experimental gerontology* 40.5 (2005), pp. 386–395.

[25] Eric Le Bourg. “Patterns of movement and ageing in Drosophila melanogaster”. In: *Archives of gerontology and geriatrics* 2.4 (1983), pp. 299–306.

[26] Eric Cook-Wiens and Michael S Grotewiel. “Dissociation between functional senescence and oxidative stress resistance in Drosophila”. In: *Experimental gerontology* 37.12 (2002), pp. 1347–1357.

[27] Giovanni Paternostro et al. “Age-associated cardiac dysfunction in Drosophila melanogaster”. In: *Circulation research* 88.10 (2001), pp. 1053–1058.

[28] Todd M Manini. “Energy expenditure and aging”. In: *Ageing research reviews* 9.1 (2010), pp. 1–11.

[29] Timothy J Doherty, Anthony A Vandervoort, and William F Brown. “Effects of ageing on the motor unit: a brief review”. In: *Canadian journal of applied physiology* 18.4 (1993), pp. 331–358.

[30] Jean-René Martin. “A portrait of locomotor behaviour in Drosophila determined by a video-tracking paradigm”. In: *Behavioural processes* 67.2 (2004), pp. 207–219.

[31] Dhruv Grover, John Tower, and Simon Tavaré. "O fly, where art thou?" In: *Journal of The Royal Society Interface* 5.27 (2008), pp. 1181–1191.

[32] Gordon J Berman et al. "Mapping the stereotyped behaviour of freely moving fruit flies Mapping the stereotyped behaviour of freely moving fruit flies". In: *J. R. Soc. Interface* 11.August (2014).

[33] Jun Nishii. "Legged insects select the optimal locomotor pattern based on the energetic cost." In: *Biological Cybernetics* 83.5 (2000), pp. 435–442.

[34] Jun Nishii. "An analytical estimation of the energy cost for legged locomotion". In: *Journal of Theoretical Biology* 238.3 (2006), pp. 636–645.

[35] Shai Revzen and John M. Guckenheimer. "Estimating the phase of synchronized oscillators". In: *Physical Review E* 78.5 (2008), pp. 1–12.

[36] S. Revzen and J. M. Guckenheimer. "Finding the dimension of slow dynamics in a rhythmic system". In: *Journal of The Royal Society Interface* 9.70 (2012), pp. 957–971.

[37] Jeffrey S Mogil. "Animal models of pain: progress and challenges." In: *Nat Rev Neurosci* 10.4 (2009), pp. 283–94.

[38] David M. Tobin et al. "Combinatorial expression of TRPV channel proteins defines their sensory functions and subcellular localization in *C. elegans* neurons". In: *Neuron* 35.2 (2002), pp. 307–318.

[39] David M. Tobin and Cornelia I. Bargmann. "Invertebrate nociception: Behaviors, neurons and molecules". In: *J Neurobiol* 61.1 (2004), pp. 161–174.

[40] Ewan St John Smith and Gary R Lewin. "Nociceptors: a phylogenetic view." In: *J Compar Physiol A, Neuroethology, sensory, neural, and behavioral physiology* 195.12 (2009), pp. 1089–1106.

[41] M. Barrot. "Tests and models of nociception and pain in rodents". In: *Neuroscience* 211 (2012), pp. 39–50.

[42] D Le Bars, M Gozariu, and S W Cadden. "Animal models of nociception." In: *Pharmacological reviews* 53.4 (2001), pp. 597–652.

[43] Fred E. D'Amour and Donn. L Smith. "A method for determining loss of pain sensation." In: *J Pharmacol Exp Ther* 72 (1941), pp. 74–79.

[44] J P O'Callaghan and S G Holtzman. "Quantification of the analgesic activity of narcotic antagonists by a modified hot-plate procedure." In: *J Pharmacol Exp Ther* 192 (1975), pp. 497–505.

[45] G. Woolfe and A. D. Macdonald. "The evaluation of the analgesic action of pethidine hydrochloride (Demerol)". In: *J Pharmacol Exp Ther* 80.3 (1944), pp. 300–307.

[46] K Hargreaves et al. "A new and sensitive method for measuring thermal nociception in cutaneous hyperalgesia." In: *Pain* 32.1 (1988), p. 11.

[47] Kirsten Wegner et al. "Development of a canine nociceptive thermal escape model". In: *Journal of Neuroscience Methods* 168.1 (2008), pp. 88–97.

[48] M Alreja et al. “The formalin test: a tonic pain model in the primate.” In: *Pain* 20.1 (1984), pp. 97–105.

[49] LA Dykstra and JH Woods. “A tail withdrawal procedure for assessing analgesic activity in rhesus monkeys.” In: *Journal of pharmacological methods* 15.3 (1986), pp. 263–269.

[50] Dale J Langford et al. “Coding of facial expressions of pain in the laboratory mouse.” In: *Nature methods* 7.6 (2010), pp. 447–449.

[51] Stephanie C J Keating et al. “Evaluation of EMLA cream for preventing pain during tattooing of rabbits: changes in physiological, behavioural and facial expression responses.” In: *PloS ONE* 7.9 (2012), e44437.

[52] Karina B Gleerup et al. “An equine pain face.” In: *Veterinary anaesthesia and analgesia* 42.1 (2015), pp. 103–114.

[53] Seol Hee Im and Michael J Galko. “Pokes, sunburn, and hot sauce: Drosophila as an emerging model for the biology of nociception.” In: *Developmental dynamics: an official publication of the American Association of Anatomists* 241.1 (2012), pp. 16–26.

[54] Takaaki Sokabe et al. “Drosophila painless is a Ca2+-requiring channel activated by noxious heat.” In: *J Neurosci* 28.40 (2008), pp. 9929–9938.

[55] Lixian Zhong, Richard Y. Hwang, and W. Daniel Tracey. “Pickpocket Is a DEG/ENaC Protein Required for Mechanical Nociception in Drosophila Larvae”. In: *Current Biology* 20.5 (2010), pp. 429–434.

[56] W Daniel Tracey et al. “Painless, a Gene Essential for Nociception”. In: *Cell* 113 (2003), pp. 261–273.

[57] Wolfgang Liedtke et al. “Mammalian TRPV4 (VR-OAC) directs behavioral responses to osmotic and mechanical stimuli in *Caenorhabditis elegans*.” In: *Proc Natl Acad Sci USA* 100 Suppl (2003), pp. 14531–14536.

[58] J V Roughan and P A Flecknell. “Effects of surgery and analgesic administration on spontaneous behaviour in singly housed rats.” In: *Research in veterinary science* 69.3 (2000), pp. 283–288.

[59] J G Culotti and R L Russell. “Osmotic avoidance defective mutants of the nematode *Caenorhabditis elegans*.” In: *Genetics* 90.2 (1978), pp. 243–256.

[60] Massimo A Hilliard et al. “Worms taste bitter: ASH neurons, QUI-1, GPA-3 and ODR-3 mediate quinine avoidance in *Caenorhabditis elegans*”. In: *EMBO J* 23.5 (2004), pp. 1101–1111.

[61] J M Kaplan and H R Horvitz. “A dual mechanosensory and chemosensory neuron in *Caenorhabditis elegans*.” In: *Proc Natl Acad Sci USA* 90.6 (Mar. 1993), pp. 2227–2231.

[62] N Wittenburg and R Baumeister. “Thermal avoidance in *Caenorhabditis elegans*: an approach to the study of nociception.” In: *Proc Natl Acad Sci USA* 96.18 (1999), pp. 10477–10482.

[63] A Mohammadi et al. "Behavioral response of *Caenorhabditis elegans* to localized thermal stimuli." In: *BMC Neuroscience* 14.1 (2013), p. 66.

[64] CI Bargmann and HR Horvitz. "Chemosensory neurons with overlapping functions direct chemotaxis to multiple chemicals in *C. elegans*." In: *Neuron* 7.5 (1991), pp. 729–742.

[65] Emily R. Troemel, Bruce E. Kimmel, and Cornelia I. Bargmann. "Reprogramming chemotaxis responses: Sensory neurons define olfactory preferences in *C. elegans*". In: *Cell* 91.2 (1997), pp. 161–169.

[66] M Huang and M Chalfie. "Gene interactions affecting mechanosensory transduction in *Caenorhabditis elegans*." In: *Nature* 367.6462 (1994), pp. 467–470.

[67] Ikue Mori and Yasumi Ohshima. "Neural regulation of thermotaxis in *Caenorhabditis elegans*". In: *Nature* 376.6538 (1995), pp. 344–348.

[68] R Ghosh et al. "Multiparameter behavioral profiling reveals distinct thermal response regimes in *Caenorhabditis elegans*". In: *BMC Biology* 10.85 (2012), p. 85.

[69] Trevor C Y Kwok et al. "A small-molecule screen in *C. elegans* yields a new calcium channel antagonist." In: *Nature* 441.7089 (2006), pp. 91–95.

[70] R Eaton and D Emberley. "How stimulus direction determines the trajectory of the Mauthner-initiated escape response in a teleost fish". In: *J Exp Biol* 161 (1991), pp. 469–487.

[71] R Eaton, DiDomenico R, and Nissanov J. "Role of the Mauthner cell in sensorimotor integration by the brain stem escape network". In: *Brain Behav Evol* 37 (1991), pp. 272–285.

[72] DA Glauser et al. "Heat avoidance is regulated by transient receptor potential (TRP) channels and a neuropeptide signaling pathway in *Caenorhabditis elegans*". In: *Genetics* 188.1 (2011), pp. 91–103.

[73] T Dezhdar et al. "A Probabilistic Model for Estimating the Depth and Threshold Temperature of C-fiber Nociceptors". In: *Sci Rep* 5 (2015), p. 17670.

[74] Greg J Stephens et al. "From modes to movement in the behavior of *Caenorhabditis elegans*." In: *PloS ONE* 5.11 (2010), e13914.

[75] S Brenner. "The genetics of *Caenorhabditis elegans*." In: *Genetics* 77.1 (1974), pp. 71–94.

[76] B Efron and R Tibshirani. *An introduction to the bootstrap*. New York: Chapman & Hall/CRC, 1994.

[77] I Nemenman and W Bialek. "Occam factors and model independent Bayesian learning of continuous distributions". In: *Phys Rev E* 65 (2002), p. 026137.

[78] Angela L Ridgel and Roy E Ritzmann. "Insights into age-related locomotor declines from studies of insects". In: *Ageing research reviews* 4.1 (2005), pp. 23–39.

[79] Donald K Ingram. "Age-related decline in physical activity: generalization to nonhumans." In: *Medicine and Science in Sports and Exercise* 32.9 (2000), pp. 1623–1629.

[80] Rachael D. Seidler et al. "Motor control and aging: Links to age-related brain structural, functional, and biochemical effects". In: *Neuroscience and Biobehavioral Reviews* 34.5 (2010), pp. 721–733.

[81] Mikael Altun et al. "Behavioral impairments of the aging rat". In: *Physiology and Behavior* 92.5 (2007), pp. 911–923.

[82] WE Trout and WD Kaplan. "A relation between longevity, metabolic rate, and activity in shaker mutants of Drosophila melanogaster". In: *Experimental gerontology* 5.1 (1970), pp. 83–92.

[83] A Navarro and A Boveris. "The mitochondrial energy transduction system and the aging process". In: *American journal of physiology Cell physiology* 292.2 (2007), pp. C670–86.

[84] RA Du Pasquier et al. "The effect of aging on postural stability: a cross sectional and longitudinal study". In: *Neurophysiologie Clinique/Clinical Neurophysiology* 33.5 (2003), pp. 213–218.

[85] Marjorie Woollacott and Anne Shumway-Cook. "Attention and the control of posture and gait: a review of an emerging area of research". In: *Gait & posture* 16.1 (2002), pp. 1–14.

[86] Fay B Horak, Charlotte L Shupert, and Alar Mirka. "Components of postural dyscontrol in the elderly: a review". In: *Neurobiology of aging* 10.6 (1989), pp. 727–738.

[87] Hylton B Menz, Stephen R Lord, and Richard C Fitzpatrick. "Age-related differences in walking stability". In: *Age and ageing* 32.2 (2003), pp. 137–142.

[88] Scott W Shaffer and Anne L Harrison. "Aging of the somatosensory system: a translational perspective". In: *Physical therapy* 87.2 (2007), p. 193.

[89] Harry B Skinner, Robert L Barrack, and Stephen D Cook. "Age-related decline in proprioception." In: *Clinical orthopaedics and related research* 184 (1984), pp. 208–211.

[90] César S Mendes et al. "Quantification of gait parameters in freely walking wild type and sensory deprived Drosophila melanogaster". In: *eLife* (2013), pp. 1–24.

[91] Robert J Wessells and Rolf Bodmer. "Screening assays for heart function mutants in Drosophila." In: *Biotechniques* 37.1 (2004), pp. 58–60.

[92] JE Fleming, I Reveillaud, and A Niedzwiecki. "Role of oxidative stress in Drosophila aging". In: *Mutation Research/DNAging* 275.3-6 (1992), pp. 267–279.

[93] Leonard Guarente and Cynthia Kenyon. "Genetic pathways that regulate ageing in model organisms". In: *Nature* 408.6809 (2000), pp. 255–262.

[94] Gabrielle L Boulianne. “Neuronal regulation of lifespan: clues from flies and worms”. In: *Mechanisms of ageing and development* 122.9 (2001), pp. 883–894.

[95] Yi-Jyun Lin, Laurent Seroude, and Seymour Benzer. “Extended life-span and stress resistance in the Drosophila mutant methuselah”. In: *Science* 282.5390 (1998), pp. 943–946.

[96] Éric Le Bourg and Nadège Minois. “A mild stress, hypergravity exposure, postpones behavioral aging in Drosophila melanogaster”. In: *Experimental gerontology* 34.2 (1999), pp. 157–172.

[97] Jamey Kain et al. “Leg-tracking and automated behavioural classification in Drosophila”. In: *Nature Communications* 4.May (2013), pp. 1910–1918.

[98] Kristin Branson et al. “High-throughput ethomics in large groups of Drosophila.” In: *Nature methods* 6.6 (2009), pp. 451–7.

[99] LH Ting, Reinhard Blickhan, and Robert J Full. “Dynamic and static stability in hexapedal runners.” In: *Journal of Experimental Biology* 197.1 (1994), pp. 251–269.

[100] R. J. Full. “Quantifying Dynamic Stability and Maneuverability in Legged Locomotion”. In: *Integrative and Comparative Biology* 42.1 (2002), pp. 149–157.

[101] Philip Holmes et al. “The Dynamics of Legged Locomotion: Models, Analyses, and Challenges”. In: *SIAM Review* 48.2 (2006), pp. 207–304.

[102] R J Full and D E Koditschek. “Templates and anchors: neuromechanical hypotheses of legged locomotion on land.” In: *The Journal of experimental biology* 202.Pt 23 (1999), pp. 3325–3332.

[103] Herman Pontzer and Richard W Wrangham. “Climbing and the daily energy cost of locomotion in wild chimpanzees: implications for hominoid locomotor evolution”. In: *Journal of human evolution* 46.3 (2004), pp. 315–333.

[104] Alexander Isakov et al. “Recovery of locomotion after injury in Drosophila melanogaster depends on proprioception”. In: *Journal of Experimental Biology* 219.11 (2016), pp. 1760–1771.

[105] Laurens van der Maaten and Geoffrey Hinton. “Visualizing data using t-SNE”. In: *Journal of Machine Learning Research* 9.Nov (2008), pp. 2579–2605.

[106] Alexander Isakov et al. “Recovery of locomotion after injury in Drosophila melanogaster depends on proprioception”. In: (2016), pp. 1760–1771.

[107] Yildirim Hurmuzlu and Cagatay Basdogan. “On the Measurement of Dynamic Stability of Human Locomotion”. In: 116.1 (1994), pp. 30–36.

[108] M J Forster et al. “Age-related losses of cognitive function and motor skills in mice are associated with oxidative protein damage in the brain.” In: *Proceedings of the National Academy of Sciences of the United States of America* 93.10 (1996), pp. 4765–9.

[109] Pei-fang Tang and Marjorie H Woollacott. "Balance Control in Older Adults: Training Effects on Balance Control and the Integration of Balance Control into Walking". In: *Advances in Psychology* 114 (1996), pp. 339–367.

[110] Lynne U Sneddon et al. "Defining and assessing animal pain". In: *Animal Behaviour* 97 (Nov. 2014), pp. 201–212.

[111] Dale J Langford et al. "Coding of facial expressions of pain in the laboratory mouse". In: *Nature methods* 7.6 (2010), pp. 447–449.

[112] Vinay Bettadapura. "Face Expression Recognition and Analysis: The State of the Art". In: *CoRR* abs/1203.6722 (2012).

[113] Chris A McGibbon and David E Krebs. "Age-related changes in lower trunk coordination and energy transfer during gait". In: *Journal of neurophysiology* 85.5 (2001), pp. 1923–1931.

[114] P. Hilber and J. Caston. "Motor skills and motor learning in Lurcher mutant mice during aging". In: *Neuroscience* 102.3 (2001), pp. 615–623.

[115] Rachael D Seidler, Jay L Alberts, and George E Stelmach. *Changes in multi-joint performance with age.* 2002.

[116] Gordon J Berman, William Bialek, and Joshua W Shaevitz. "Predictability and hierarchy in Drosophila behavior". In: *Proceedings of the National Academy of Sciences* 113.42 (2016), pp. 11943–11948.